The ARF GAP ELMOD2 acts with different GTPases to regulate centrosomal microtubule nucleation and cytokinesis

Rachel E. Turn[a,b], Michael P. East[c], Rytis Prekeris[d], and Richard A. Kahn[a,*]
[a]Department of Biochemistry, Emory University School of Medicine, Atlanta, GA 30322; [b]Biochemistry, Cell & Developmental Biology Graduate Program, Laney Graduate School, Emory University, Atlanta, GA 30307; [c]Department of Pharmacology, University of North Carolina Chapel Hill, Chapel Hill, NC 27599; [d]Department of Cell and Developmental Biology, University of Colorado, Aurora, CO 80045

ABSTRACT **ELMOD2 is a ~32 kDa protein first purified by its GTPase-activating protein (GAP) activity toward ARL2 and later shown to have uniquely broad specificity toward ARF family GTPases in in vitro assays. To begin the task of defining its functions in cells, we deleted ELMOD2 in immortalized mouse embryonic fibroblasts and discovered a number of cellular defects, which are reversed upon expression of ELMOD2-myc. We show that these defects, resulting from the loss of ELMOD2, are linked to two different pathways and two different GTPases: with ARL2 and TBCD to support microtubule nucleation from centrosomes and with ARF6 in cytokinesis. These data highlight key aspects of signaling by ARF family GAPs that contribute to previously underappreciated sources of complexity, including GAPs acting from multiple sites in cells, working with multiple GTPases, and contributing to the spatial and temporal control of regulatory GTPases by serving as both GAPs and effectors.**

Monitoring Editor
Benjamin Glick
University of Chicago

Received: Jan 7, 2020
Revised: Apr 21, 2020
Accepted: Jun 24, 2020

INTRODUCTION

To carry out essential cellular processes, a cell requires diverse cellular compartments to communicate and synchronize with one another. Cell division alone requires DNA replication and condensation, nuclear envelope breakdown, mitochondrial fragmentation, actin and microtubule cytoskeletal rearrangement, centrosome duplication and migration, ciliary resorption, and many other events to be performed and timed correctly to facilitate the generation of two new cells. It stands to reason that there must be signaling network(s) to allow for these discrete processes to communicate. Regulatory GTPases are strong candidates as keys to such communication and integration of cellular processes because of their ability to act from multiple locations and with different partners and regulators in the same cells. The ARF superfamily of regulatory GTPases (in mammals represented by six ARFs, 22 ARLs (ARF-like proteins), and two SARs [Sztul *et al.*, 2019]) is one such example not only because many of the members localize to diverse cellular compartments and work with multiple different effectors, but also because they are ancient (most members found in eukaryotes were predicted to have been present in the last eukaryotic common ancestor), very highly conserved, and ubiquitous in eukaryotes (Li *et al.*, 2004; Klinger *et al.*, 2016; Sztul *et al.*, 2019).

While the ARFs are best known for their roles in the regulation of membrane traffic (Kahn *et al.*, 2005; D'Souza-Schorey and Chavrier, 2006; Jackson and Bouvet, 2014), ARF family GTPases are also critical regulators of a diverse array of essential cellular functions (Nie *et al.*, 2003; Burd *et al.*, 2004; D'Souza-Schorey and Chavrier, 2006; Gillingham and Munro, 2007; Donaldson and Jackson, 2011; Seixas *et al.*, 2013). In several instances, single members of this family regulate multiple processes at distinct sites, making dissection and

This article was published online ahead of print in MBoC in Press (http://www.molbiolcell.org/cgi/doi/10.1091/mbc.E20-01-0012) on July 2, 2020.

Declaration of interests: We do not have any conflicts of interest to disclose.

Author contributions: R.E.T. designed, performed, and analyzed experiments and prepared figures. M.P.E. provided critical training for CRISPR-Cas9 technologies. R.P. provided critical insight into experimental design and model-building. R.E.T. and R.A.K. developed this study and prepared the manuscript. All authors reviewed the findings and edited and approved the final version.

*Address correspondence to: Richard A. Kahn (rkahn@emory.edu). ORCID 0000-0002-0259-0601.

Abbreviations used: BSA, bovine serum albumin; FBS, fetal bovine serum; GAP, GTPase-activating protein; GEF, guanine nucleotide exchange factor; ICB, intercellular bridge; KO, knockout; MEF, mouse embryonic fibroblast; PCM, pericentriolar material; PBS, phosphate-buffered saline; PFA, paraformaldehyde; TBC, tubulin-specific chaperone; WT, wild type.

elucidation of each molecular pathway challenging (Francis *et al*., 2016; Sztul *et al*., 2019). In other cases, multiple family members share overlapping or redundant functionalities, making clear demonstrations of the role(s) of any one a challenge (e.g., ARF1–3 all share >96% identity, overlapping localization, and common binding partners). A further complication to clear understanding of any one signaling pathway is that the proteins tasked with turning off these GTPases, the ARF GTPase-activating proteins or ARF GAPs, are also almost always effectors, contributing to the propagation of the signal from the GTPase to a biological response (Zhang *et al*., 1998, 2003; Inoue and Randazzo, 2007; East and Kahn, 2011; Vitali *et al*., 2019). While a challenge to researchers, the ability of one cell regulator to act on multiple essential cellular processes and at distinct sites has also been posited to provide an important means of communication between those functions and between the distinct cellular locations from which they act (East and Kahn, 2011; Sztul *et al*., 2019).

Multiplicity of functions at distinct locations is perhaps most clearly demonstrated for ARL2. It is found predominantly in a cytosolic, heterotrimeric complex with TBCD and β-tubulin (Bhamidipati *et al*., 2000; Shultz *et al*., 2008; Francis *et al*., 2017a) but also localizes to centrosomes (Zhou *et al*., 2006), mitochondria (Newman *et al*., 2014, 2017a), and rods and rings (Schiavon *et al*., 2018). Genetic screens in multiple model organisms identified ARL2 and TBCD orthologues as key players affecting microtubules and cell division (McElver *et al*., 2000; Radcliffe *et al*., 2000; Antoshechkin and Han, 2002; Price *et al*., 2010). Stearns *et al*. (1990) identified mutants in *Saccharomyces cerevisiae* of ARL2 (*CIN4*) and TBCD (*CIN1*) based on supersensitivity to benomyl, while a related screen linked mutations in these same genes to increased chromosome loss and defects in nuclear migration and nuclear fusion (Hoyt *et al*., 1990). Nick Cowan's group discovered five cofactors required for tubulin heterodimer formation (termed tubulin-specific chaperones A–E; TBCA–E [Tian *et al*., 1996]) and first posited a specific role for ARL2 working with TBCD in a tubulin folding pathway (Tian *et al*., 2010). An obligate role for ARL2 in the folding of the αβ-tubulin heterodimer was later expanded upon with structural studies (Francis *et al*., 2017a,b). Other studies suggest a role for ARL2 and TBCD in microtubule polymerization, acting from centrosomes (Zhou *et al*., 2006; Cunningham and Kahn, 2008). ARL2 was later shown to mediate mitochondrial fusion from the inner membrane space (Sharer *et al*., 2002; Newman *et al*., 2014, 2017a; Schiavon *et al*., 2019). Still other studies have revealed roles for ARL2 in transport of farnesylated cargoes to the transition zone of primary cilia (Ismail *et al*., 2011; Watzlich *et al*., 2013), in STAT3 signaling in the nucleus (Muromoto *et al*., 2008), and as a component of rods and rings (Schiavon *et al*., 2018). That one protein regulates so many pathways and from so many different locations highlights the complexity involved in generating models of its actions at any one site. Yet, it offers the promise of important insights into cell regulation with better models of the mechanisms that drive interpathway communication.

Another example of diversity in function by one ARF family member is ARF6. This GTPase is found at the plasma membrane, cytoplasm, cleavage furrows, and Flemming bodies (D'Souza-Schorey *et al*., 1995; Cavenagh *et al*., 1996; Hosaka *et al*., 1996). ARF6 facilitates membrane and actin remodeling, and activated ARF6 is recruited to the cleavage furrow where it supports ingression in early cytokinesis (Radhakrishna and Donaldson, 1997; D'Souza-Schorey *et al*., 1998; Frank *et al*., 1998; Song *et al*., 1998). Depletion of ARF6 leads to failures in cytokinesis (Schweitzer and D'Souza-Schorey, 2002, 2005; Makyio *et al*., 2012; Ueda *et al*., 2013). Other studies have revealed the importance of its binding to MKLP1 at the Flemming body in the completion of cytokinesis (Takahashi *et al*., 2011; Makyio *et al*., 2012; Ueda *et al*., 2013; Hanai *et al*., 2016), where it is predicted to either mediate the traffic of key factors to and from the midbody to facilitate the proper docking of endosomes or to promote the recruitment of FIP3 (Takahashi *et al*., 2011).

Like the ARF superfamily, the family of ARF GAPs is also highly conserved and ancient (Schlacht *et al*., 2013), with 24 genes/proteins in mammals that all share the ARF GAP domain (Randazzo *et al*., 2007; Spang *et al*., 2010; Donaldson and Jackson, 2011; East and Kahn, 2011; Sztul *et al*., 2019; Vitali *et al*., 2019). However, these ARF GAPs have consistently been shown to act only on the six ARFs and not on the ARLs. In contrast, ELMOD2 was purified based on its GAP activity toward ARL2 and later was shown to act in vitro on both a number of ARLs and ARFs (Bowzard *et al*., 2007; Ivanova *et al*., 2014). There are three ELMOD family members (ELMOD1–3) in mammals that share a common ELMO domain with the three ELMO proteins (ELMO1–3), though only the ELMODs have GAP activities for ARFs and ARLs (Bowzard *et al*., 2007; East *et al*., 2012). Thus, ELMODs have uniquely broad substrate specificity that includes several GTPases tested in the ARF family; these include ARL1, ARL2, ARL3, ARF1, and ARF6 but not ARL13B (Bowzard *et al*., 2007; Ivanova *et al*., 2014). The ELMOD family is also ancient, predicted to have been present in the last eukaryotic common ancestor (East *et al*., 2012), and linked to various pathologies; these include idiopathic pulmonary fibrosis (ELMOD2 [Hodgson *et al*., 2006]), deafness (ELMOD1 and ELMOD3 [Johnson *et al*., 2012; Li *et al*., 2018, 2019], intellectual disability (ELMOD1 and ELMOD3 [Miryounesi *et al*., 2019; Loi *et al*., 2020]), and antiviral response (ELMOD2 [Pulkkinen *et al*., 2010]). The broad specificity of ELMODs for GTPases in the ARF family in in vitro GAP assays increases the likelihood that the ELMODs work with multiple (currently unknown) GTPases in cells. This promiscuity makes teasing apart the biological functions of ELMODs more complicated to dissect and makes ELMODs more likely to serve key roles in multiple pathways.

The cellular functions and specificity of ELMODs as GAPs in cells have not yet been characterized. These proteins are expressed only to low levels, making their detection and quantification challenging. Of the three, ELMOD2 displayed the highest in vitro GAP activities (Ivanova *et al*., 2014) and has been localized to mitochondria, the endoplasmic reticulum (ER), and lipid droplets. Yet, functions at these locations have been shown for only ELMOD2 and ARL2 acting from the intermembrane space to regulate mitochondrial fusion (Schiavon *et al*., 2019). Here, we used CRISPR-Cas9 to generate frameshifting/null mutations of ELMOD2 in immortalized mouse embryonic fibroblasts (MEFs). These lines not only proved useful earlier for gaining mechanistic insight into ELMOD2's role(s) in mitochondrial fusion (Schiavon *et al*., 2019), but they also revealed a host of unexpected phenotypes that were not apparent from previous knockdown or overexpression studies. Our data highlight both the importance of this protein to two essential cellular processes and the complexities involved in dissecting signaling by ARF GTPases and their interactors.

RESULTS

With the goal of identifying cellular functions for ELMOD2, we generated cell lines specifically deleted for ELMOD2. We used CRISPR-Cas9 genome editing to introduce frame-shifting mutations of both alleles in MEFs, as described earlier (Schiavon *et al*., 2019). By targeting close to the 5′ end of the open reading frame and upstream of the sole, catalytic ELMO domain (Supplemental Figure S1A), we expect that any protein fragments made from the mutated ELMOD2 gene will be inactive, as well as potentially rapidly degraded. We

will refer to such lines herein as null or knockout (KO) lines, even though a short N-terminal peptide might exist in cells. To strengthen any conclusions drawn from characterization of these lines and specifically to protect against off-target effects that can occur from CRISPR, we generated multiple cell lines from two different guide RNAs. A total of 10 independently cloned KO lines was obtained (Supplemental Figure S1B). Screening of cell lines was performed by genomic DNA sequencing after PCR amplification of the region targeted. We also generated a lentivirus that directs expression of mouse ELMOD2 with a C-terminal myc epitope (ELMOD2-myc) and used it to transduce our MEF lines to further strengthen the link between any observed phenotypes and the loss of cellular ELMOD2. Clones found to have no changes in the targeted exon are referred to as "CRISPR WT" and are retained as controls, as they have been through the same transfection, selection, and cloning processes as the nulls. We narrowed down the number of test samples to include four KO lines (KO #4, 6, 8, and 10; see Supplemental Figure S1), the same four KO lines after transduction with virus to drive expression of ELMOD2-myc, two wild-type (WT) lines (one parental population, one CRISPR WT), and the same two WT lines expressing ELMOD2-myc. Hereafter, we will refer to these cells as the "12 standard lines." Finally, we note that every phenotype described below was evident in all 10 KO lines when tested and differed only in the magnitude of the changes. These are typically shown as the range, with more detailed analyses performed on the 12 standard lines.

We screened ELMOD2 null lines using markers of various cellular compartments both to assess potential global changes in organelle morphology as well as to specifically look for changes in compartments to which ELMOD2 had been localized (i.e., mitochondria and lipid droplets). As predicted and demonstrated earlier, we observed mitochondrial defects (fragmentation) consistent with ELMOD2 acting with ARL2 in mitochondrial fusion (Schiavon *et al.*, 2019). In contrast, staining of WT and ELMOD2 null cells with BODIPY, either untreated or after a 24 h exposure to 30 mM oleic acid, showed no changes in the number or size of lipid droplets that might be ascribed to the deletion of ELMOD2 (Supplemental Figure S2). These early, broad screens did reveal a number of other cellular changes to result from deletion of ELMOD2 that we describe and analyze further below.

ELMOD2 null MEFs display multiple defects linked to microtubules

During routine handling and culture of ELMOD2 null cells, we observed some obvious differences from WT cells, for example, in cell morphology. Cell rounding was evident in each of our 10 ELMOD2 null lines and appeared to correlate with time spent out of the 37°C incubator, at room temperature, but was not seen in WT or rescued lines. Cell rounding can result from defects in any of several different processes. Given the established links between ELMOD2 and ARL2, though, as well as the roles of ARL2 and its partner TBCD in tubulin heterodimer assembly, microtubule stability, γ-tubulin ring complex (γ-TuRC) recruitment, and links to chromosome instability, we hypothesized that the cold sensitivity of ELMOD2 null MEFs was tied to the changes in microtubules (Hoyt *et al.*, 1990; Zhou *et al.*, 2006; Bowzard *et al.*, 2007; Ivanova *et al.*, 2014; Francis *et al.*, 2017a; Newman *et al.*, 2017b).

A time course study revealed that changes in cell morphology became evident within 1 min at room temperature, progressing and persisting for at least 2 h. Approximately 50% of cells became rounded within the first 15 min, and those that did not remained flat for at least 2 h. We chose 15 min for more detailed analyses as a time at which changes were prominent in null cells but not in WT. Cells were removed from the incubator and either fixed immediately or after 15 min at room temperature (~22°C). Tubulin staining was not obviously different in WT and null cells fixed immediately upon removal from the incubator; microtubules fill the majority of the cell body and are ordered in appearance (Figure 1A). Quantification revealed that the percentage of cells with depleted microtubule networks was slightly increased in KO (17.1%) compared with controls (3.3%; $p < 0.05$; Figure 1B). In contrast, within 15 min at room temperature, ELMOD2 KOs displayed a pronounced loss of microtubule staining compared with WT MEFs (77.8% in KO lines vs. 8.8% in WT lines; Figure 1, A and B). This is evident from the loss of overall microtubule staining and less frequent evidence of their organization around a centrosome in the nulls (see Supplemental Figure S4 for details on binning of microtubule density). In marked contrast, there was little or no evidence of changes in the microtubule network of WT cells between the 0 and 15 min time points (Figure 1, A and B). Quantification of loss of microtubule networks (Figure 1B) included scoring of both rounded and flat cells, as rounded cells were also depleted of microtubules. While both WT and null cells display loss of microtubules and cell rounding at 4°C, these changes are initiated more rapidly and are more evident in the null lines (unpublished data). Thus, ELMOD2 nulls clearly display an increased cold sensitivity for microtubules. Expression of ELMOD2-myc in nulls resulted in the near complete rescue of cold sensitivity, in that cell rounding and microtubule network densities each reverted to near WT levels (Figure 1, A and B [KO+D2]). Expression of ELMOD2-myc in WT cells had no apparent effect on either parameter (Figure 1A).

Changes in microtubule sensitivity can also be assessed through their response to drugs that act on microtubules, such as nocodazole, as previously used in genetic screens in model organisms (Hoyt *et al.*, 1990; Stearns *et al.*, 1990). Nocodazole sensitivity was assessed in the 12 standard lines, grown to ~70% confluence, after treatment with increasing concentrations of nocodazole (0–100 ng/ml) for 2 h, followed by fixation and staining for α-tubulin, as described under *Materials and Methods*. Cell rounding occurred in response to nocodazole, and such cells lacked evidence of, or had a greatly reduced, microtubule network. WT cells begin demonstrating clear evidence of microtubule loss at 5–10 ng/ml nocodazole and are most sensitive to changes in the drug at these concentrations, under these conditions (Figure 1C). In contrast, comparable loss of microtubules was evident in ELMOD2 KO cells with as little as 2 ng/ml nocodazole (Figure 1C). At 5 ng/ml, ELMOD2 KO cells have more than threefold more cells displaying loss of microtubules (average of WT = 18.5%, range 13.5–23.5%; average of KO = 63.1%, range 59.5–66.75%). The expression of ELMOD2-myc in rescued lines reversed the nocodazole supersensitivity of ELMOD2 null MEFs (average = 17.1%, range 15.75–18.5%) but had no effect on WT cells. At 20 ng/ml, all 12 lines presented with 100% of cells with microtubule loss (Figure 1C). Thus, the absence of ELMOD2 in MEFs causes the microtubule network to become more sensitive to both cold and nocodazole.

ELMOD2 localizes to centrosomes, and its deletion causes delay in the recruitment of γ-TuRC and in microtubule nucleation from centrosomes

Microtubule network organization, regulation, and function(s) rely on a variety of different factors. Increased sensitivity to cold and nocodazole could be the product of increased microtubule catastrophe, delays in microtubule nucleation, changes in pools of polymerizable tubulin, altered microtubule anchorage, or other

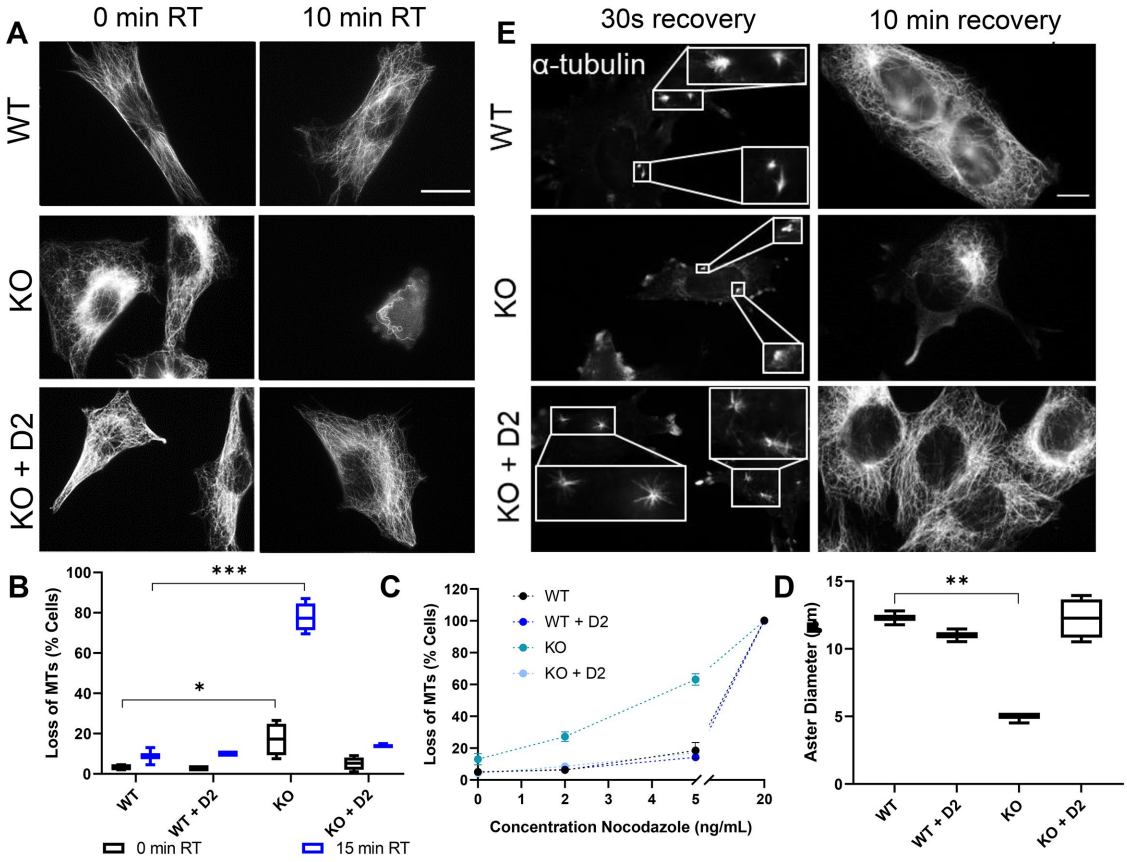

FIGURE 1: Loss of ELMOD2 leads to decreased microtubule stability. (A) Microtubules in ELMOD2 null MEFs display increased cold sensitivity compared with WT cells. Cells grown at the same densities were fixed either immediately after removal from the incubator (left panels) or after 15 min at room temperature (~23°C; right panels), before staining for α-tubulin. Representative images collected via widefield microscopy at 100× magnification are shown. Scale bar = 10 μm. (B) Our 12 standard lines imaged as described in A and scored for obvious loss in microtubule densities, as described under *Materials and Methods*. For each cell line, 100 cells were scored in duplicate and averaged. WT, $N = 2$ lines; WT + D2 (WT cells expressing ELMOD2-myc), $N = 2$; KO (ELMOD2 nulls), $N = 4$; KO + D2 (ELMOD2 nulls expressing ELMOD2-myc), $N = 4$. Statistical significance was assessed using two-way ANOVA; *** = $p < 0.0001$. (C) ELMOD2 KO lines show increased sensitivity to nocodazole. The effects of increasing concentrations of nocodazole (0–100 ng/ml) on microtubule networks are shown for the different cell lines. Cells were stained for α-tubulin and scored for microtubule networks. Error bars represent the SEM, after scoring 100 cells in duplicate. Two-way ANOVA statistical analysis reveals that KO cells have significantly ($p < 0.0001$) increased nocodazole sensitivity at 2 and 5 ng/ml. WT, $N = 2$ lines; WT + D2 (WT cells expressing ELMOD2-myc), $N = 2$; KO (ELMOD2 nulls), $N = 4$; KO + D2 (ELMOD2 nulls expressing ELMOD2-myc), $N = 4$. (D) Aster formation is delayed in ELMOD2 null MEFs after nocodazole washout. Cells were incubated with nocodazole (50 ng/ml) for 2 h, drug was washed out, and cells were fixed 30 s later and stained for α-tubulin and γ-tubulin (nunpublished data). Cells were imaged at 100× magnification on a widefield microscope, and images were taken of random fields of cells. A minimum of 50 asters were imaged for each of the 11 lines tested ($N = 2$ WT, 2 WT + D2, 3 KO, 4 KO + D2) in duplicate. Aster diameters were measured with FIJI software. Note that differences in KO lines are larger than they appear in this graph, as we did not score α-tubulin–negative centrosome staining at this early time point after release from drug; these were clearly more numerous in KO lines. (E) Asters were imaged at either 30 s or 10 min after washout of nocodazole, as described in panel D. Asters are boxed and shown at higher magnification for ready comparison. Statistical significance was assessed using one-way ANOVA; ** = $p < 0.01$. Scale bar = 10 μm.

means. To begin narrowing in on the role of ELMOD2, we used the aster formation assay (Cunningham and Kahn, 2008) to assess the rate of microtubule polymerization from centrosomes. We treated cells with 50 ng/ml nocodazole (optimized to increase the number of cells with complete microtubule loss while minimizing toxicity) for 2 h, before replacing the drug with fresh medium and monitoring the formation of asters by staining fixed cells for tubulin. The cells were fixed at time points up to 20 min after release from nocodazole; the 30 s and 10 min time points are shown in Figure 1E. Cells were stained for α- and γ-tubulin to track aster formation. Both WT and null cells showed at least some asters at the earliest time point (30 s after nocodazole washout). However, the rate at which asters grow or new asters appear was clearly slower in the null lines (Figure 1, D and E; $p < 0.001$). Scoring of this assay is described further in Supplemental Figure S5. We also noted the presence of more than two asters in some ELMOD2 null cells, resulting from microtubule nucleation from supernumerary centrosomes (see below). By 10 min, WT cells have recovered microtubule arrays and cell morphology comparable to untreated cells. ELMOD2 nulls also have restored microtubule networks, though their networks are less ordered,

emanate less obviously from centrosome-nucleated asters, and frequently do not extend to the cell periphery (Figure 1E, 10 min recovery).

The presence of microtubules but lack of an obvious microtubule organizing center in many ELMOD2 null cells recovering from nocodazole prompted us to ask whether nucleation of new microtubule growth was specifically defective at centrosomes and perhaps retained at other sites (e.g., Golgi or plasma membrane [Tassin *et al.*, 1985a,b; Chabin-Brion *et al.*, 2001; Bugnard *et al.*, 2005; Efimov *et al.*, 2007; Zhu and Kaverina, 2013; Rios, 2014; Petry and Vale, 2015; Wu and Akhmanova, 2017]). Therefore, cells were incubated on ice for 30 min to deplete the microtubule network and then returned to 37°C for different times before fixation with 4% paraformaldehyde (PFA), permeabilization with 0.1% Triton X-100, and staining for α-tubulin and γ-tubulin. At 0 min recovery from cold exposure, both WT and ELMOD2 null cells presented with a greatly depleted microtubule network, showing little or no evidence of a centrosomal microtubule organizing center. Peripheral microtubules were still present in both WT and null cells and at similar levels, though the microtubules were clearly less organized than in untreated cells. At each time point of recovery from cold, peripheral microtubules in both WT and null cells appeared to recover at indistinguishable rates. Cells fixed immediately after cold exposure show little to no γ-tubulin–positive centrosomes. In both WT and KO cells, the majority of the cells show background, punctate γ-tubulin staining, but no obvious bright foci consistent with centrosomes (Figure 2A). This indicates that the cold treatment used here causes at least partial changes in γ-tubulin, and thus γ-TuRC, at centrosomes, or more specifically at the pericentriolar material (PCM). After 5 min of recovery from cold, the vast majority (87.5%; range 83–92%; Figure 2B) of WT cells show the return of γ-tubulin–positive centrosomes. In contrast, our KO lines show delayed recovery, with an average of only 21.3% (range 13–29%; Figure 2B) of cells showing γ-tubulin at centrosomes with 5 min recovery. Rescue with ELMOD2-myc in null

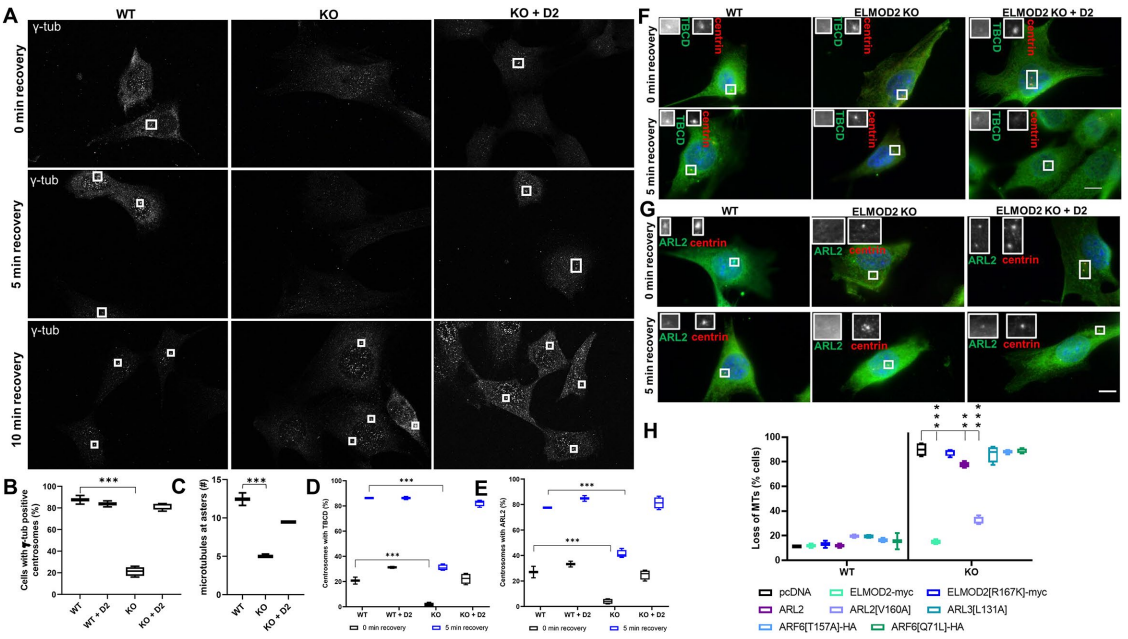

FIGURE 2: ELMOD2 nulls are slow to recruit γ-TuRC, ARL2, and TBCD to centrosomes during recovery from cold. Cells were incubated on ice for 30 min to deplete the microtubule network, and then returned to 37°C and fixed at different times during recovery before being stained for γ-tubulin to mark centrosomes. (A) Widefield images shown (100× magnification) are representative of the number of cells displaying γ-tubulin–positive centrosomes. (B) Scoring of the percentage of cells with γ-tubulin–positive centrosomes was performed, as described under *Materials and Methods*, after 5 min recovery. Statistical significance was assessed using one-way ANOVA; *** = $p < 0.0001$. (C) Two WT, three KO, and two rescued lines were fixed after 5 min of recovery from cold and stained for α- and γ-tubulin. *Z*-stacks were collected. These images were analyzed using FIJI software, and the microtubules protruding from each centrosome were manually counted from each layer of the *z*-stack. The cut-off for what was considered a microtubule (using the FIJI measuring tool) was 0.5 µm. The *z*-section with the largest number of microtubules protruding from the centrosome was recorded, and the average of these values for each cell line is shown, as described under *Materials and Methods*. Statistical significance was assessed using one-way ANOVA; *** = $p < 0.0001$. (D–G) Cells were fixed using ice-cold methanol and stained for centrin and ARL2 or TBCD, as described under *Materials and Methods*, at either 0 or 5 min of recovery at 37°C from cold exposure. Widefield imaging was used to score for centrin (to mark centrosomes) and ARL2 or TBCD. (D, E) The standard 12 cell lines were scored in duplicate experiments with 100 cells per condition and averaged. Statistical significance was assessed using two-way ANOVA; *** = $p < 0.0001$. (F, G) Representative widefield images at 100× magnification are shown. (H) Two WT and four ELMOD2 KO lines were transfected with either empty vector (pcDNA) or the same vector directing expression of ELMOD2-myc, ELMOD2[R167K]-myc, ARL2 ARL2[V160A], ARL3[L131A], ARF6[T157A]-HA, or ARF6[Q71L]-HA, as indicated. The next day, cells were maintained at room temperature for 15 min prior to fixation and staining for α-tubulin and either myc, ARL2, ARL3, or HA to identify transfected cells. Densities of microtubule networks of transfected cells were scored in duplicate and averaged, as described under *Materials and Methods*. Statistical significance was assessed using one-way ANOVA; *** = $p < 0.0001$. Scale bar = 10 µm. Only expression of ELMOD2-myc, ARL2, or ARL2[V160A] significantly reversed microtubule cold sensitivity in KO cells.

cells reversed this effect to near WT levels (82.6%; range 76–88%). By 10 min, γ-tubulin–positive centrosomes have recovered in practically all cells.

This loss or delay in γ-tubulin recruitment to centrosomes after cold was also accompanied by a decrease in the number of microtubules emanating from them even after its return. We quantified the number of microtubules at γ-tubulin–positive centrosomes, as described under *Materials and Methods* and illustrated in Supplemental Figure S6, at the 5 min time point. While WT cells had an average of 12.4 microtubules (range 11.6–13.2) at γ-tubulin–positive centrosomes, the four KO lines had an average of 5.1 (range 5.0–5.3) microtubules. These four rescue lines showed numbers approaching those seen in wild-type cells (average 9.5 microtubules, range 9.4–9.6; Figure 2C). Note that in this assay we scored only cells with γ-tubulin–positive centrosomes and because we earlier found that KO lines show loss or delay in return of γ-tubulin to centrosomes, these data underestimate the severity of the differences in microtubules at asters during recovery from cold.

Taken together, these data point to a role for ELMOD2 in the recruitment of γ-tubulin, and by extension γ-TuRC, to centrosomes. However, ELMOD2 has not previously been localized to centrosomes. We had earlier generated rabbit polyclonal antibodies directed against ELMOD2 and used them to demonstrate localization in mitochondria (Newman *et al.*, 2017b). Others have reported its presence at lipid droplets using proteomics or immunoblotting of purified preparations as well as exogenous expression of tagged protein (Bouchoux *et al.*, 2011; East *et al.*, 2012; Suzuki *et al.*, 2015). Previous immunofluorescence experiments with our ELMOD2 antibody used fixation with PFA and permeabilization with saponin or Triton X-100, which are conditions often used to visualize antigens in or on membranous compartments. However, protein dense structures like centrosomes and midbodies typically do not immunostain well under those conditions. Rather, it is common to fix and permeabilize in cold methanol, as described under *Materials and Methods*. WT MEFs were stained with our rabbit polyclonal antibody to ELMOD2 along with markers of microtubules (α-tubulin) and centrosomes (γ-tubulin) (see Figure 5A later in this article). These studies revealed specific staining of ELMOD2 at both centrosomes and Flemming bodies, though not at cleavage furrows or the intercellular bridge (ICB) of midbodies (similar to ARL2, which also localizes to both centrosomes and Flemming bodies [Supplemental Figure S3]). ELMOD2 staining was strongly decreased or completely absent from centrosomes and midbodies when the primary antibody was first incubated with purified GST-ELMOD2 (i.e., antigen competition). In addition, staining of ELMOD2 at centrosomes and Flemming bodies was not observed in KO lines. These two important controls for immunostaining confirm the specific localization of endogenous ELMOD2 to centrosomes and midbodies in MEFs and provide novel potential sites at which it may act to alter microtubule dynamics or cytokinesis (see below) when deleted.

Previous data from our lab revealed a role for ARL2 and its binding partner TBCD in γ-TuRC anchoring (Cunningham and Kahn, 2008) and for ARL2 binding ELMOD2 (Bowzard *et al.*, 2007; Ivanova *et al.*, 2014). Thus, we also asked whether deletion of ELMOD2 affected the localization/recruitment of ARL2 or TBCD to centrosomes under cold stress. Using the same conditions for recovery from cold described above, cells were costained for centrin (to mark centrioles) and for either ARL2 or TBCD, as described under *Materials and Methods*. At each time point, centriolar staining of centrin is evident in all our cell lines, suggesting that cold exposure does not disrupt its localization to centrioles. In contrast, we observed loss of ARL2 and TBCD in response to cold stress in all cells, though this effect was more pronounced in the KO lines than in WT or rescued lines. Upon 0 min recovery from cold, 20.8% of WT cells were positive for TBCD staining at centrosomes (range 16–24%) and 27% were positive for ARL2 at centrosomes (range 21–35%). In contrast, 1.8% of KO cells displayed TBCD staining at centrosomes (range 0–4%) and 4% had ARL2 (range 0–8%). The decreased TBCD and ARL2 recruitment is reversed upon rescue with ELMOD2-myc, 21.3% (range 14–30%) and 25% (range 18–30%), respectively. After 5 min of recovery, 86.3% of centrosomes in WT cells were positive for TBCD (range 85–88%) and 77.5% for ARL2 (range 74–81%), while only 31.1% of null cells had TBCD (range 24–40%) and 41.3% (range 38–47%) had ARL2. This decrease in ARL2 and TBCD recruitment in ELMOD2 null cells, compared with WT, was reversed upon expression of ELMOD2-myc as we found 82.4% of null cells positive for TBCD (range 77–89%) and 81.3% (range 73–88%) for ARL2. By 10 min of recovery from cold, both ARL2 and TBCD staining recovered at centrosomes in both WT and KO cells. Thus, the loss of ELMOD2 in MEFs causes instability in the binding of γ-TuRC, ARL2, and TBCD at centrosomes in response to cold stress and delays in their ability to be recruited back to centrosomes during recovery from cold. We noted a small but statistically significant ($p < 0.01$) increase in the percentages of WT cells retaining centrosomal TBCD after cold (0 min recovery) when expressing ELMOD2-myc, as well as an elevated percentage of centrosomes retaining ARL2, though the latter is not statistically significant. This is consistent with a model in which ELMOD2 is a key component in regulating the recruitment of these two other proteins, though clearly requires more detailed study. Deletions of these other proteins or live cell imaging and determining the kinetics of each of them under different stressors may provide important insights into the ordering of recruitment but was deemed beyond the scope of the current study. However, because ELMOD2 was identified as an ARL2 GAP, we pushed our analyses in this direction further, in efforts to assess 1) whether ELMOD2 is acting as a GAP in these responses, 2) whether increasing ARL2 activity can reverse effects seen in the absence of ELMOD2, and 3) if so, whether this effect is specific to ARL2.

Reversal of cold sensitivity by ELMOD2 requires its GAP activity or activated ARL2

Because ARF GAPs can function in cells as both terminators of GTPase signaling and as effectors of those same GTPases, we tested whether expression of the previously described (East *et al.*, 2012) GAP dead mutant, ELMOD2[R167K], rescues the cold-sensitive phenotype that we described above. We note that the mitochondrial fragmentation that occurs in MFN1 null MEFs is reversed upon expression of either WT or GAP dead ELMOD2, which supports the model that ELMOD2 acts as an effector of ARL2 inside mitochondria (Schiavon *et al.*, 2019). As seen in Figure 2H, expression of ELMOD2-myc reverses the effects of ELMOD2 deletion on cold sensitivity of microtubules. Two WT and four KO lines were transiently transfected with a pCDNA3.1-based vector either "empty" (serving as negative control) or directing expression of ELMOD2[R167K]-myc. The following day, cells were fixed and stained for α-tubulin and myc both immediately after removal from the incubator and after a 15 min incubation at room temperature. No differences were found between scoring of cold sensitivity–induced changes in tubulin staining in untransfected cells (unpublished data), those transfected with empty vector, or those expressing ELMOD2[R167K]-myc (Figure 2H). Thus, GAP activity appears to be required for the actions of ELMOD2 that impact microtubule densities and cold sensitivity of cell morphology.

If the GAP activity of ELMOD2 is required for reversal of cold sensitivity, we reasoned that increasing the activity of the GTPase that it is working with in this pathway may also reverse the effects resulting from ELMOD2 deletion. Though ELMOD2 was purified as an ARL2 GAP, it was later shown to be promiscuous and to act on multiple ARF family GTPases (including both ARLs and ARFs) using in vitro GAP assays (Bowzard *et al.*, 2007; Ivanova *et al.*, 2014). Within the ARF family, only ARL2 and its closest paralogue, ARL3, have been linked to microtubules (Zhou *et al.*, 2006). We asked whether cold sensitivity of microtubules could be rescued by increasing the activity of either GTPase through expression of activating mutants. The dominant, activating mutant ARL2[Q70L] has previously been shown to cause strong and irreversible effects on microtubules and other structures in CHO cells (Zhou *et al.*, 2006; Newman *et al.*, 2014). We saw similar strong effects of ARL2[Q70L] in MEFs, with essentially complete loss of microtubules in all expressing cells (unpublished data). We were concerned that such strong effects would prove difficult to sort out from those resulting from loss of ELMOD2. This mutant is analogous to RAS[Q61L] (Chipperfield *et al.*, 1985; Adari *et al.*, 1988) or ARF1[Q71L] (Zhang *et al.*, 1994), as each is activating as a result of the loss of GTP hydrolysis and thus cannot inactivate the GTPases. An alternative means of generating activating GTPases is to increase the rate limiting step in their *activation* (release of bound GDP) via mutation of a conserved threonine. This residue lies in the nucleotide binding pocket making direct contact with the guanine ring (Santy, 2002; Aspenstrom, 2018) and is situated in the highly conserved "T(C/S)AT" or G-5 motif. The site is T157 in ARF6 and is homologous to V160 in ARL2 and L131 in ARL3. Such mutants were first described in RAS and RHO GTPases (Reinstein *et al.*, 1991; Lin *et al.*, 1997, 1999; Fidyk *et al.*, 2006; Aspenstrom, 2018). Santy later demonstrated the utility of analogous mutants of ARF6 (Santy, 2002), and this was later extended to other family members (Moravec *et al.*, 2012; D'Souza *et al.*, 2020). These mutants increase the turnover of the activation/deactivation cycle and are thus also referred to as "fast cycling" activating mutants and, importantly here, remain sensitive to GAPs. Therefore, they can be more informative than the Q to L mutants, which are locked into only the activated conformation, preventing cycling.

Expression of fast cycling ARL2 (ARL2[V160A]) in WT MEF lines caused little or no changes to the microtubule network and thus offered a means of attempting rescue with this activating mutant (Figure 2H; average 19.5%, range 18–21%). The cold-sensitive microtubule loss in ELMOD2 null lines (Figure 2H; average 89.8%, range 84.5–95%) was strongly reversed upon expression of ARL2[V160A] in each of the four KO lines assayed (Figure 2H; average 31.9%, range 29.5–36.5%, $p < 0.0001$) to almost the same extent as seen with ELMOD2-HA. Even wild-type ARL2 has a small ability to reverse the loss of microtubules ($p < 0.01$). In contrast, expression of activating mutants of other ARF family GTPases (ARL3 [ARL3[L131A]], ARF6 [ARF6[T157A]], and the dominant activated ARF6 [ARF6[Q71L]]) had no effect on the microtubule defects in ELMOD2 KO lines (Figure 2H). Thus, ARL2 is uniquely capable of rescuing the microtubule defects seen in ELMOD2 null MEFs. This result is consistent with ELMOD2 and ARL2 acting in a single common pathway, or perhaps two parallel pathways, that influence microtubule stability.

KO lines are multinucleated and polyploid and have supernumerary centrosomes

While performing the experiments described above, it was evident that other things were aberrant in our KO lines that seemed to point to dysfunction in some aspect of cell division. These included apparent increases in the number of centrosomes, evident when staining for γ-TuRC or centrin, and multinucleation, evident from Hoechst staining. So, we next set out to quantify these effects and test whether they are consequences of the changes in microtubules, described above, or separate pathways that may also have a requirement for ELMOD2.

We saw no consistent differences in rates of cell proliferation correlating with genotype while cloning the KO lines or during routine maintenance of them. However, simply staining for DNA (with Hoechst) revealed a large increase in the incidence of multinucleation in ELMOD2 KO lines. All 10 KO lines were analyzed (technical triplicates of 100 cells counted per line) for nuclear number, and we found that an average of 17.1% (range of 10 lines 10.0–20.3%) of ELMOD2 KO cells have two or more nuclei, compared with 1.6% of WT cells (range 1.3–2.0%; Figure 3A). This experiment was scored in triplicate but was repeated many times with consistent results, as we routinely stain for Hoechst in immunocytochemistry experiments. Although we use the term multinucleation, the clear majority of multinucleated cells are binucleated.

Multinucleation was largely reversed upon expression of ELMOD2-myc (Figure 3A; $p < 0.0001$). While the average percentage of multinucleated cells in our standard KO lines was 20.6% (range 20.0–21.3%), this was reduced to 5.0% (range 3.3%–6.7%) after expression of ELMOD2-myc. Because lentivirus infection efficiency was between 70 and 90% (positive for myc staining), scoring was performed for all cells. As a result, the presence of at least 10% of cells in the culture that do not express ELMOD2-myc is expected to at least partially account for the incomplete rescue. Thus, it is evident that multinucleation is a common phenotype observed in cells lacking ELMOD2 that is reversed upon its reintroduction.

To assess DNA content, we used flow cytometry with propidium iodide staining of DNA. The 12 standard lines were each analyzed in technical triplicate. The six other null lines were each analyzed at least once, with none displaying results that deviated clearly from the data summarized here. Even without cell synchronization, null lines often presented with an increased G2/M (4N) peak compared with WT cells, and often also displayed 8N peaks (Figure 3B). These results are consistent with a subpopulation of null cells being either multinucleated or polyploid. To better assess the nature of the lesion, cells were synchronized using a double thymidine block followed by nocodazole to maximize the number of cells in G2/M (4N), as described under *Materials and Methods*. After synchronization, an 8N population of cells emerged in all null lines and was quite prominent in several of them (Figure 3B). Because the apparent percentage of cells with 8N is clearly in excess of the percentage of multinucleated cells (~20%; Figure 3C), we conclude that polyploidy is not occurring exclusively in mononucleated cells. While multinucleation was reversed upon expression of ELMOD2-myc in KO lines, this was not the case for polyploidy. Reversal of polyploidy may require more time than does multinucleation, as cells do not have a known mechanism for removing excess DNA. All the data reported herein use low passage numbers (<10) to minimize the impact of phenotypic drift over time.

Multinucleation is often the result of failure in cytokinesis and frequently is associated with an increased incidence of supernumerary centrosomes. To examine centrosome numbers, cells were plated at ~70% confluence, fixed the next day, and stained for two markers of centrosomes: γ-tubulin and centrin. The two WT lines displayed an average of 98.9% of cells having one or two centrosomes, or 1.1% having more than two centrosomes (Figure 3C). In marked contrast, in the 10 KO lines, an average of 25.0% of cells

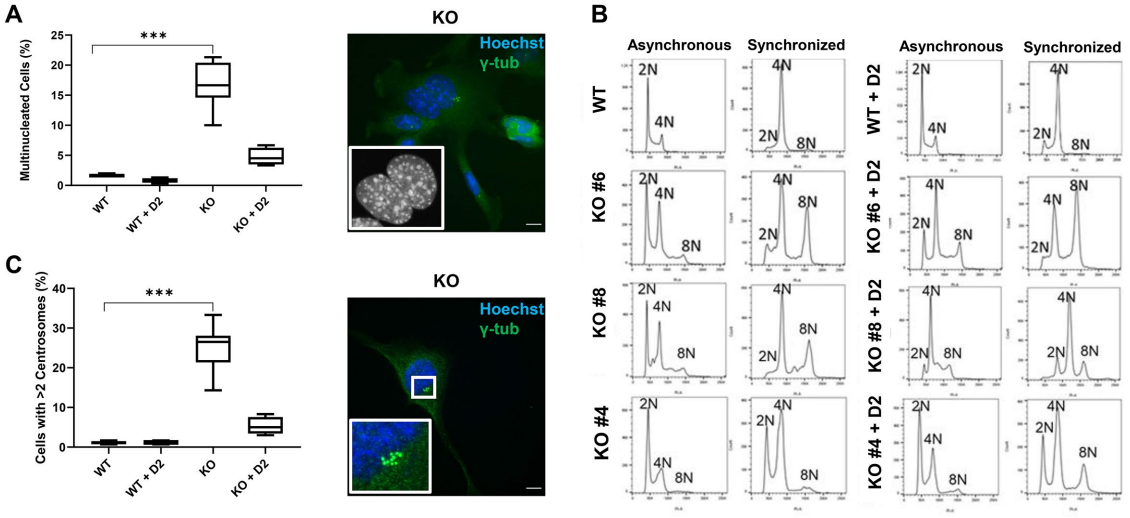

FIGURE 3: Deletion of ELMOD2 causes multinucleation, supernumerary centrosomes, and polyploidy. (A) Multinucleation was assessed by plating cells from four WT, two WT lines expressing ELMOD2-myc (WT+D2), 10 KO, and four KO lines expressing ELMOD2-myc (KO + D2), fixing the next day, staining for Hoechst to mark nuclei, and scoring the number of cells with two or more nuclei. Percent multinucleation was quantified in triplicate (100 cells per replicate) for all lines analyzed, with data being graphed as box-and-whisker plots. Statistical significance was assessed using one-way ANOVA; *** = $p < 0.0001$. A representative confocal (100× magnification, *z*-projection) image of ELMOD2 null (KO) cells is shown on the right. Inset shows higher magnification and grayscale to highlight the two nuclei in the cell shown. Scale bar = 10 μm. (B) DNA content is increased in cells deleted for ELMOD2. Flow cytometry was used to quantify DNA content in at least 10,000 cells per condition, after staining with propidium iodine, as described under *Materials and Methods*. Both unsynchronized (left panels) and synchronized (double thymidine plus nocodazole block) (right panels) were analyzed. DNA content from WT (top panels) and three different KO lines are shown as graphs in the left set of panels. The panels on the right show the DNA content of the same four lines after transduction with ELMOD2-myc. Graphs were generated using FloJo software, as described in *Materials and Methods*. (C) Cells plated at approximately 70% density were assessed for centrosome numbers after staining for γ-tubulin, centrin, and Hoechst. Averages of tri plicate determinations for each of the lines tested are shown. Statistical significance was assessed using one-way ANOVA; *** = $p < 0.0001$. An image from a KO line, taken via confocal microscopy at 100× magnification, *z*-projected, is shown on the right. Scale bar = 10 μm.

had more than two centrosomes (Figure 3C; range = 14.3–29.3%; $p < 0.0001$). The majority of these cells have three to four centrosomes, though some cells had as many as 20 centrosomes. All multinucleated cells displayed supernumerary centrosomes, but not all cells with supernumerary centrosomes were multinucleated. The number and arrangement of centrosomes appeared to vary widely from cell to cell (e.g., there was no obvious trend in centrosomes being clustered, and there was no obvious preference for even numbers of centrosomes). This phenotype was largely reversed upon expression of ELMOD2-myc in all four KO lines tested, as the average in these four lines dropped from 27.1% to 5.3% post-transduction. Because both these phenotypes are reversed upon expression of ELMOD2-myc, multinucleation and centrosome amplification result from the loss of ELMOD2 and not from potential off-target effects of CRISPR-Cas9.

ELMOD2 null cells display higher rates of cytokinesis failures

Multinucleation, polyploidy, and centrosome amplification can each result from defects in cell division. We sought to determine whether a specific stage in cell division is compromised in cells lacking ELMOD2. Our 12 standard lines were imaged by brightfield microscopy over 24 h at 37°C, capturing *z*-projections every 10 min (Figure 4A). We observed no failures in cell division in WT cells. In contrast, ELMOD2 null cells frequently displayed defects in the later stages of cell division that included late failure in cytokinesis: the cells generated a midbody, but they were incapable of completing abscission (Figure 4A, top row). We also noted common instances in which cells complete cytokinesis with apparently normal nuclear division, but the cells take a markedly prolonged time to complete cytokinesis (Figure 4A, bottom row). To gain a better perspective, as well as increase the numbers of cells analyzed at specific points in the cell cycle, we continued these studies using fixed synchronized cell populations.

Cells were treated with the CDK1 inhibitor RO-3306 (7.5 μg/ml) for 18 h to block cells at the beginning of mitosis. The drug was removed, and cells were fixed at time points up to 5 h before staining for α-tubulin, γ-tubulin, and Hoechst to track mitotic indices and cell division (see *Materials and Methods* and Supplemental Figure S7). WT cells displayed a wave of cell divisions with clearly increased mitotic indices within 10 min of drug removal, peaking at 20 min at an average of 42.5% mitotic cells, followed by lower mitotic indices (9–16% on average) throughout the remainder of the 5 h imaging window (Figure 4B). ELMOD2 nulls had a similar onset of increased mitotic index and achieved a maximum average of 51.3% 30 min after release from inhibitor. In contrast to WT cells that had a short-lived peak in mitotic indices, this level plateaued and was sustained at ≥40% of cells throughout most of the 5 h time course in KO lines. Mitotic indices of ELMOD2 nulls never returned to the levels seen in WT MEFs, even 5 h after release from CDK1 inhibitor (32.5%). Thus, the lack of ELMOD2 results in long delays in completion of cytokinesis. This result is consistent with the live cell imaging data, as the most common defects observed were either stalling or failure at late cytokinesis.

Consistent with delays in completion of cytokinesis, both synchronized and unsynchronized ELMOD2 null lines display a higher percentage of cells with midbodies (as visualized by α-tubulin

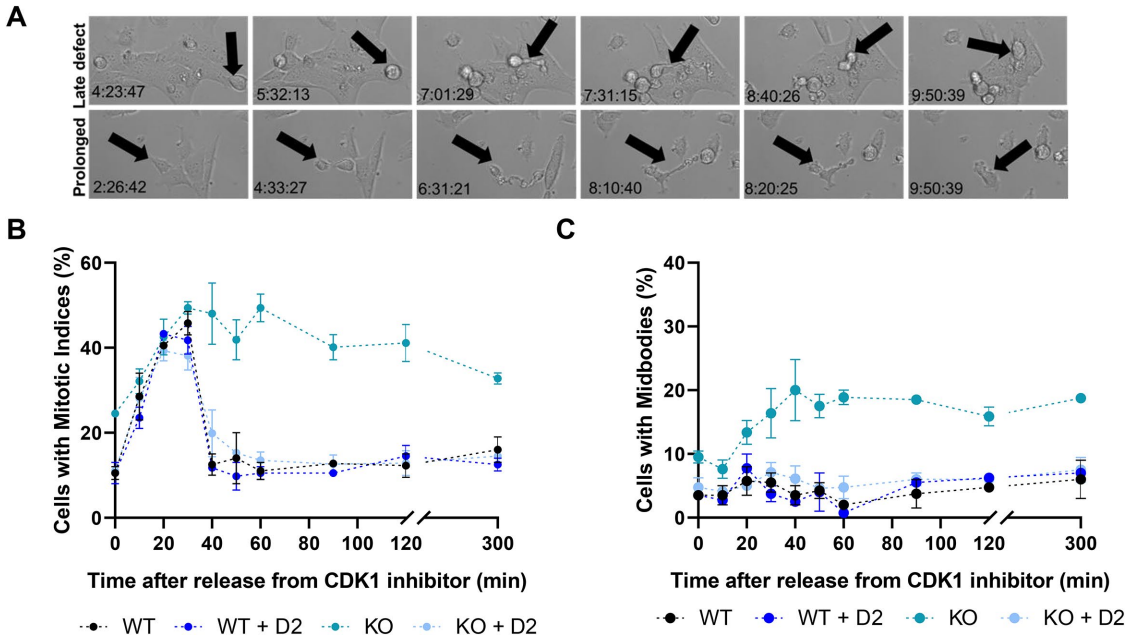

FIGURE 4: ELMOD2 null cells display a prolonged cytokinesis and both early and late cytokinesis defects. (A) Panels from time-lapse imaging collected from unsynchronized cells reveal cytokinesis defects in ELMOD2 nulls. Phase-contrast images at 40× magnification were collected every 10 min using a Lionheart FX (BioTek) microscope. Images were selected to highlight defects observed, with time points indicated in the bottom left. (B) Cells were synchronized by treatment with CDK1 inhibitor (RO-3306; 7.5 μg/ml) for 18 h; the drug was washed out, and cells were fixed at the time points indicated in the graphs. Cells were stained for α-tubulin, γ-tubulin, and Hoechst and visualized via widefield microscopy to track cells during stages of the cell cycle. Cells were binned into prophase, metaphase, anaphase, telophase, or late cytokinesis, as described in *Materials and Methods* (see Supplemental Figure S7). These experiments were performed in triplicate, 100 cells per replicate, using the standard 12 lines. Ranging from 40 to 120 min after release from CDK1 inhibitor, KO cells show significantly ($p < 0.0001$) increased mitotic indices compared with WT. This increase in mitotic indices persists even up to 300 min after release ($p < 0.05$, measured by one-way ANOVA). (C) The same samples described in panel B were scored for the presence of midbodies as markers of late cytokinesis, consistent with stalling late in cell division. Starting at 40 min after release from CDK1 inhibitor, KO lines have significantly ($p < 0.01$) higher percentages of cells with midbodies than do WT (by one-way ANOVA).

staining). At no time point after washout of the drug did WT MEFs have more than 6.5% of cells with a midbody throughout the 5 h imaging window. In contrast, the average of the four KO lines was a maximum of ~20% of cells with midbodies, and this is maintained throughout the 5 h imaging window (Figure 4C). The increased fraction of cells displaying midbodies was also accompanied by an increase in the number of very long midbodies and midbody remnants (residual midbodies that persist after abscission). Remarkably, there were also instances in which one cell was attached to two others via distinct midbodies. These were each uncommon (estimated at 1% but not rigorously quantified), though never observed in WT lines. Expression of ELMOD2-myc in WT lines had little to no effect on the percentage of cells with midbodies at any time point but was sufficient to return the percentage of cells with midbodies in ELMOD2 null lines nearly to WT levels (Figure 4C). Together, these data support a role for ELMOD2 in late cytokinesis, though defects at other stages have not been excluded.

ELMOD2 null MEFs have reduced recruitment of ARF6 to midbodies

The later stages of cytokinesis, including abscission, require the selective recruitment of multiple regulatory proteins to key sites (including centrosomes, cleavage furrows, recycling endosomes, and midbodies) via mechanisms that are often incompletely understood (Agromayor and Martin-Serrano, 2013; Nakayama, 2016; Nahse *et al*., 2017; Peterman and Prekeris, 2019). Such proteins may traffic to the mitotic spindle or cleavage furrow during metaphase and anaphase, and later to specific parts of the midbody to facilitate abscission. Some inconsistency in terminology exists in the literature. So, to be clear, we refer to the entire structure that bridges two dividing cells as the midbody, which consists of two ICBs on either side of a central Flemming body. We sought to better define potential sites and mechanisms of ELMOD2 action to tease apart its role(s) in cytokinesis. We monitored the recruitment and retention of a number of other components at these sites at different stages in the cell cycle, with the aim of determining whether ELMOD2 can be linked to any known cytokinesis pathways. We focused on both markers of the key compartments/processes as well as on proteins previously linked to ARF family GTPases. Sixteen endogenous proteins were localized in WT and ELMOD2 null MEFs (plated at the same density) using cold methanol fixation and specific antibodies directed against ARL1, ARL2, ARL3, ARFs (monoclonal 1D9), ARF6, RHOA, RAB11, RAB11-FIP3 (hereafter termed FIP3), MKLP1, α- and γ-tubulin, acetylated tubulin, centrin, BART/ARL2BP, TBCD, and ELMOD2, as described under *Materials and Methods*. A summary of localizations observed for these proteins in MEFs is shown in Figure 5B.

Almost all previously described markers of the Flemming body (e.g., MKLP1, RHOA, and FIP3 [Supplemental Figure S1A]) and ICB (α-tubulin, γ-tubulin, acetylated tubulin, and RAB11 [Supplemental Figure S3B]) localize indistinguishably in WT and ELMOD2 null cells. We have previously shown ARL3, TBCD, and BART to localize to the Flemming body, and these, too, were unaltered in ELMOD2 null

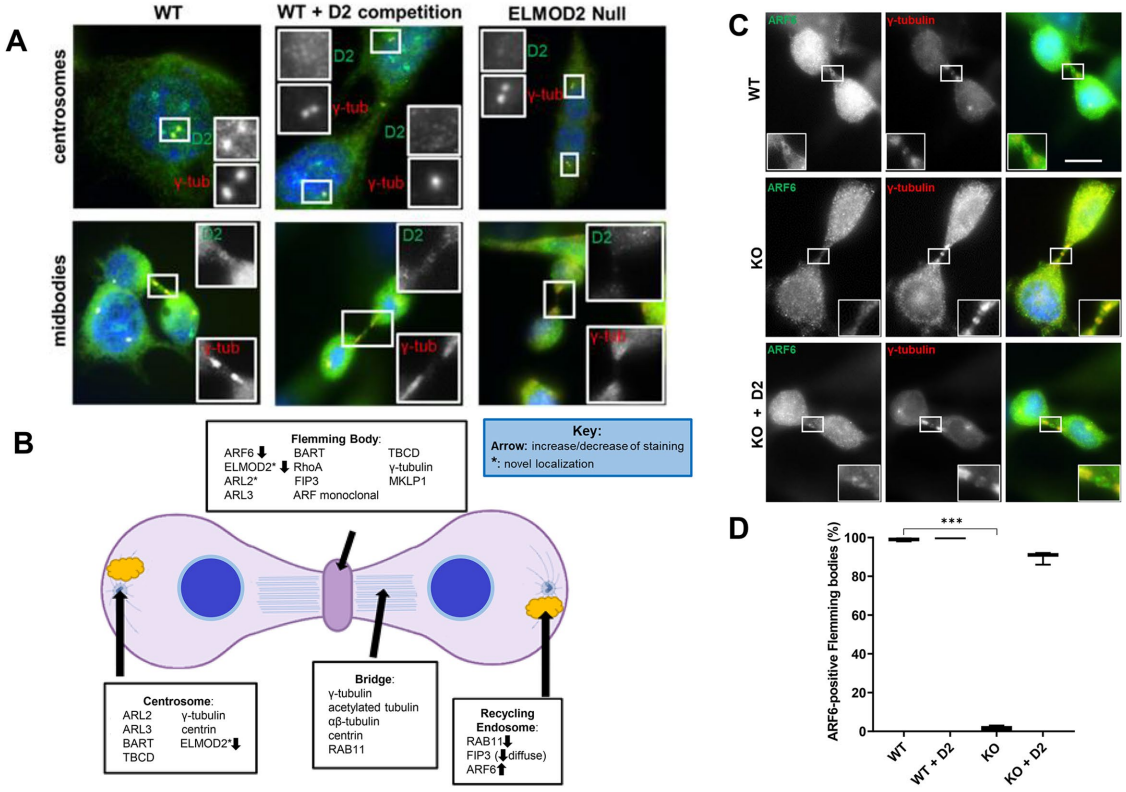

FIGURE 5: ARF6, RAB11, and FIP3 are specifically altered in localization in ELMOD2 null cells. (A) Localization of ELMOD2 at centrosomes (top panels) and midbodies (bottom panels) was identified via immunocytochemistry after methanol fixation (see *Materials and Methods*). Cells were stained for γ-tubulin (red), ELMOD2 (green), and Hoechst (blue). Antigen competition (WT + D2 competition) involved prior incubation of the ELMOD2 antibody with purified ELMOD2 protein, as described under *Materials and Methods*, and is shown in the center panels. Specificity of ELMOD2 staining at these sites was further supported as staining is lost in null cells, shown in panels on the right. (B) Summary of the 16 different markers of centrosomes, midbodies, Flemming bodies, and endosome clusters tested is shown. Black arrows indicate either increases or decreases in staining of these markers, and a black asterisk indicates a novel localization of the protein at the site indicated. (C) Widefield images (100× magnification) of methanol-fixed cells stained for ARF6 and γ-tubulin reveal that ARF6 staining at midbodies is lost in null cells but is recovered upon rescue with ELMOD2-myc. Scale bar = 10 μm. (D) The number of ARF6-positive Flemming bodies was quantified for two WT, two WT + D2, four KO, and three KO + D2 lines in duplicate (50 midbodies per replicate). The duplicates for each line were averaged, and results were tabulated in box-and-whisker plots in GraphPad Prism. Statistical significance was assessed using one-way ANOVA; *** = $p < 0.0001$.

MEFs compared with WTs. ARL2 has not previously been localized to the Flemming body, but it also is unaltered in staining in both WT and null MEFs (Supplemental Figure S3C). ARL2, ARL3, and TBCD staining at centrosomes appears unchanged in null versus WT cells, though as noted above, cold stress does promote the release of ARL2 and TBCD to a greater extent in KO than WT cells.

In marked contrast, ARF6 is no longer found at the Flemming body of ELMOD2 nulls (Figure 5, C and D). This loss of ARF6 staining is reversed upon expression of ELMOD2-myc. We examined four KO lines, and ARF6 was absent from Flemming bodies in each case, while staining of ARF6 was restored in every case upon expression of ELMOD2-myc (Figure 6D; $p < 0.0001$). Thus, the loss of ELMOD2 in cells and from Flemming bodies is accompanied by the specific loss of ARF6 from Flemming bodies.

ELMOD2 nulls show reduced RAB11 and increased ARF6 recruitment to FIP3-GFP–positive endosomes

To begin to test the model that ELMOD2 is acting with ARF6 to mediate cytokinesis, we next checked to see whether other factors in this pathway were disrupted by loss of ELMOD2. Prior to their recruitment to midbodies, ARF6, RAB11, and FIP3 are each recruited to recycling endosomes adjacent to centrosomes (Prigent *et al.*, 2003; Schiel *et al.*, 2012). From there, ARF6 traffics to the cleavage furrow to facilitate furrow ingression, and later to the Flemming body during cytokinesis. RAB11 and FIP3 are recruited to the ICB. Just before abscission, it is thought that FIP3 moves from the ICB to the Flemming body, where ARF6 has already been recruited (Schiel *et al.*, 2012). Their location at the Flemming body is critical for the final stages of abscission. To visualize these processes, we used FIP3-GFP expression to identify the relevant recycling endosomes and to follow changes in localization of these key proteins at these sites, as previously described (Schiel *et al.*, 2012).

Expression of FIP3-GFP in WT cells results in bright staining (Figure 6A, top panel) of a cluster that was shown previously to be recycling endosomes adjacent to or surrounding the centrosome (Schiel *et al.*, 2012). In a small subset (<10%) of WT cells, we also observed evidence of a diffuse GFP signal as well as a mixture of clustered and diffuse staining, quantified in Figure 6B. Cells expressing FIP3-GFP were also stained with antibodies to FIP3 and yielded the same results, arguing against GFP being cleaved from FIP3 and confusing interpretations. The FIP3-GFP recycling endosomal clusters also stained strongly for RAB11, though cytosolic staining of

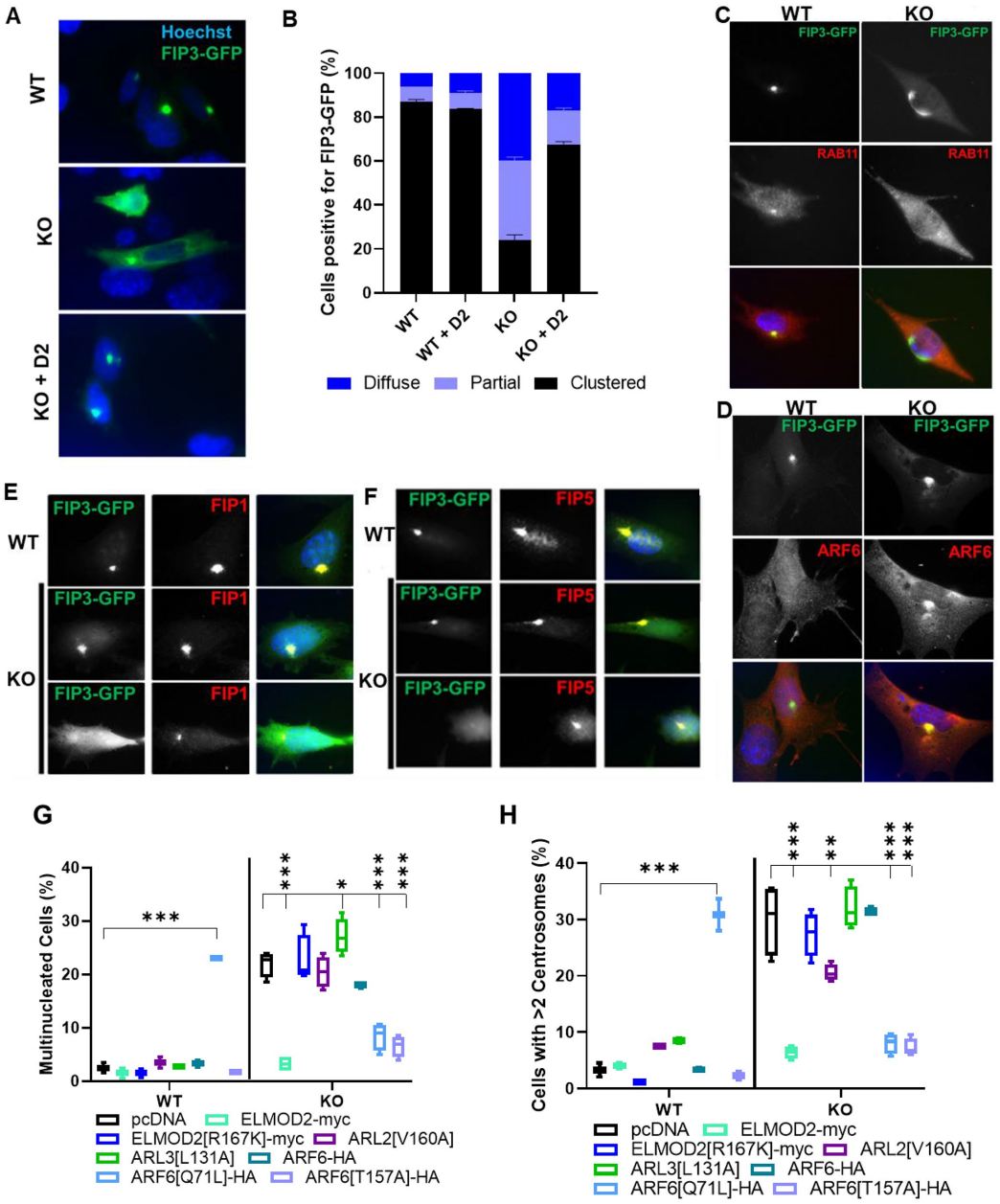

FIGURE 6: ELMOD2 KO cells display decreased recruitment of FIP3-GFP, along with loss of RAB11 and increases in ARF6 at recycling endosome clusters. (A) Standard lines were transfected with FIP3-GFP (green) to visualize recycling endosome clusters. Cells were fixed with methanol and stained for Hoechst (blue), as described in *Materials and Methods*. Fluorescence images were collected via widefield microscopy at 100× magnification. Note the loss of clustering (one more complete than the other) in the two cells expressing FIP3-GFP shown in the middle panel and the phenotypic reversal with expression of ELMOD2-myc (bottom panel). (B) The experiment described in panel A was scored in triplicate (100 cells each); results were binned into either complete clustered, partial clustered/partial diffuse, or completely diffuse staining of FIP3-GFP. Error bars represent the SEM of the cell lines scored for each genotype. Two-way ANOVAs show that complete and partially diffuse FIP3-GFP staining are increased in null lines compared with WT ($p < 0.0001$). (C–F) Representative images of 100× magnification widefield images were collected to determine colocalization of RAB11, ARF6, and FIP1/5 (each shown in red), with FIP3-GFP (green)-positive clusters. Scale bar = 10 μm. (G, H): GAP dead ELMOD2 cannot reverse the cytokinesis defects in ELMOD2 null cells but activated ARF6 specifically does. Cells from two WT and four KO lines were transfected with either empty vector or the same vector directing expression of ARL2[V160A], ARL3[L131A], ARF6-HA, ARF6[Q71L]-HA, ARF6[T157A]-HA, ELMOD2-myc, or ELMOD2[R167K]-myc. The next day, samples were fixed with methanol and stained for myc, γ-tubulin, and Hoechst. Multinucleation (G) and supernumerary centrosome (H) were scored in transfected cells, as described under *Materials and Methods*. These experiments were performed and analyzed in triplicate (100 cells per replicate), and the averages of each are shown, with lines representing the SEM. Statistical significance was assessed using one-way ANOVA. Only the following were found to be statistically significant: ARL3[L131A] increased multinucleation, ARL2[V160A] decreased supernumerary centrosomes, ARF6[Q71L]-HA increased both multinucleation and centrosome numbers in WT cells and decreased both in KO cells, and ARF6[T157A]-HA reversed both phenotypes; *** = $p < 0.0001$.

RAB11 was also always evident (Figure 6C). We repeated this experiment several times with different WT lines and always obtained the same results. We also investigated ARF6 localization to recycling endosomes. WT cells expressing FIP3-GFP display ARF6 staining that is diffuse/cytosolic, with little to no evidence of enrichment at FIP3-positive clusters over background (Figure 6D).

In contrast, FIP3-GFP staining was much more diffuse in all four ELMOD2 null lines analyzed (Figure 6, A and B). A subpopulation (<30%) of these cells retain a strong GFP signal at clusters with little diffuse staining, while another ~30% show retention of a clear cluster but with obvious, diffuse staining. The remainder (~40%) have only diffuse GFP signal (all quantified in Figure 6B). In ELMOD2 null lines, there is a uniform and pronounced loss of RAB11 staining at recycling endosomes, regardless of whether FIP3-GFP is clustered (Figure 6C). This effect is quite strong, though occasionally a weak RAB11 signal can still be seen to costain FIP3-GFP clusters. The partial or complete loss of FIP3-GFP clustering and of RAB11 costaining at recycling endosomes was reversed upon expression of ELMOD2-myc in all four rescued lines.

All members of the FIP family (RAB11-FIP1 through 5) bind to and are recruited to endosomes in concert with RAB11, though only FIP3 and FIP4 bind to ARF6 (Hickson *et al.*, 2003; Fielding *et al.*, 2005; Wilson *et al.*, 2005; Horgan and McCaffrey, 2009). As a test of the specificity of FIP family members being sensitive to the loss of ELMOD2, we immunostained FIP3-GFP transfected cells for FIP1 or FIP5. FIP3-GFP–positive clusters in WT cells stain positive for both FIP1 and FIP5 (Figure 6, E and F), and this staining was not altered upon deletion of ELMOD2. Furthermore, even in ELMOD2 null cells with diffuse FIP3-GFP staining, FIP1 and FIP5 are still recruited to clusters. This suggests that FIP1 and FIP5 localization to endosomes is unaffected by the loss of ELMOD2, and thus the effect is specific to the ARF6 binder FIP3.

In contrast to WT cells, in which ARF6 staining at FIP3-GFP clusters was either faint or not evident, our ELMOD2 nulls displayed uniformly strong ARF6 staining at recycling endosome clusters (Figure 6D). This increased ARF6 staining was reversed upon expression of ELMOD2-myc in KO lines. Thus, loss of ELMOD2 results in compromised FIP3-GFP clustering, no changes in FIP1 or FIP5 clustering, (near) complete loss of RAB11, and strong increases in ARF6 at that site. These data lead us to propose a model in which RAB11 and ARF6 compete for the binding of FIP3 at recycling endosomes (see *Discussion*).

ELMOD2 GAP activity is required for rescue of multinucleation and centrosome amplification

Having identified a novel role for ELMOD2 in cell division, we next sought to understand the mechanism(s) by which ELMOD2 mediates cytokinesis. To determine whether ELMOD2 is acting as a GAP in cytokinesis, we transfected the standard two WT and four KO lines with a plasmid directing expression of ELMOD2[R167K]-myc to determine whether it could reverse supernumerary centrosomes and multinucleation, as shown previously for ELMOD2-myc (see above). Cells were transfected, fixed 48 h later, and stained for myc, γ-tubulin, and Hoechst, as described under *Materials and Methods*. WT MEFs expressing the GAP-dead ELMOD2 appeared normal in morphology (e.g., mononucleated, one to two centrosomes) with only an average of 1.5% of cells being multinucleated and 1.2% of cells having supernumerary centrosomes (Figure 6, G and H). KO lines that express ELMOD2[R167K] display comparable levels of multinucleation (22.7%) and supernumerary centrosomes (27.4%) as empty vector controls (19.3% and 27.6%, respectively) or untransfected ELMOD2 nulls (17.1% and 25.0%, respectively). Because we showed above that ELMOD2-myc reverses multinucleation and centrosome amplification but the GAP dead point mutant shows virtually no such rescue, we conclude that, in contrast to ELMOD2's role with ARL2 in mitochondrial fusion (Schiavon *et al.*, 2019) but like its role in microtubules, GAP activity *is* required for its function(s) in these processes.

Expression of activated ARF6-HA rescues cytokinesis defects seen in ELMOD2 null MEFs

Given the prior evidence demonstrating effects of ARF6 mutants on endosomes and cell division (e.g., (D'Souza-Schorey *et al.*, 1998; Donaldson and Radhakrishna, 2001), we hypothesized that ELMOD2 may act as a GAP to inactivate ARF6 at recycling endosomes to mediate cytokinesis. This could explain the accumulation of ARF6 at FIP3-GFP–positive endosome clusters, if inactivation of ARF6 is required for its release from that site. To begin to address such a model, we expressed ARF6-HA, dominant activating point mutant (ARF6[Q67L]-HA), or empty vector control into the standard 12 cell lines. Cells were fixed 48 h later, stained, and scored for multinucleation and centrosome amplification, as described in *Materials and Methods*. Neither transfection controls (empty vector) nor expression of ARF6-HA resulted in changes in the extent of multinucleation (2.0% and 3.3%, respectively) or centrosome amplification (2.3% and 3.3%, respectively) in WT cells (Figure 6, G and H, respectively). In contrast, expression of ARF6[Q67L]-HA in WT cells led to large increases in both multinucleation (average = 23.0%; Figure 6G; $p < 0.0001$) and supernumerary centrosomes (30.8%; Figure 6H; $p < 0.0001$), consistent with the consequences of excessive ARF6 activity to the cell cycle, as previously reported (Schweitzer and D'Souza-Schorey, 2002). The effects of increased ARF6 activity in WT cells are comparable to the consequences of deletion of ELMOD2 (17.1% multinucleation, range of 10–21.3%, and 25.0% centrosome amplification, range of 14.3–33.3%, respectively [Figure 6, G and H]).

Multinucleation and centrosome amplification in ELMOD2 nulls were unaffected by transfection (empty vector) or expression of ARF6-HA (19.3% and 18.0% multinucleation; and 27.6% and 31.4%, supernumerary centrosomes, respectively) (Figure 6, G and H). In marked contrast, expression of ARF6[Q67L]-HA resulted in substantial reversal of both multinucleation and supernumerary centrosome defects in ELMOD2 nulls (8.4% multinucleation; 8.0% supernumerary centrosomes [Figure 6, G and H]).

Though ARF6[Q67L]-HA can rescue the defects seen in ELMOD2 nulls, the fact that it causes multinucleation and supernumerary centrosome defects in WT cells complicates interpretations. Similar effects of ARF6[Q67L] on midbodies and cytokinesis have been reported in HeLa and Jurkat cells (Schweitzer and D'Souza-Schorey, 2002). To further examine the role of ARF6 in cells deleted for ELMOD2, we used the same rationale described above in use of fast cycling ARL2 to rescue changes in microtubules. The corresponding activating mutation in ARF6 is ARF6[T157A]-HA, and we compared it to ARF6[Q71L] in both WT and KO lines. Interestingly, only ARF6[Q71L]-HA caused increases in multinucleation in WT cells; ARF6[V160A]-HA did not (multinucleation: average 1.75%, range 1.5–2.0%; supernumerary centrosome: average 2.25%, range 1.5–3%) (Figure 6G). This is consistent with the ARF6[Q71L] mutant "locking" its pathway in an activated state and preventing cycling. In doing so, this mutant may actually be inhibiting the pathway, perhaps analogous to that seen upon depletion of ARF6 (Schweitzer and D'Souza-Schorey, 2005). While ARF6[T157A]-HA does not cause multinucleation in WT cells, it is as effective as ARF6[Q71L]-HA in reversing the effects of ELMOD2 deletion (Figure 6H; $p < 0.0001$),

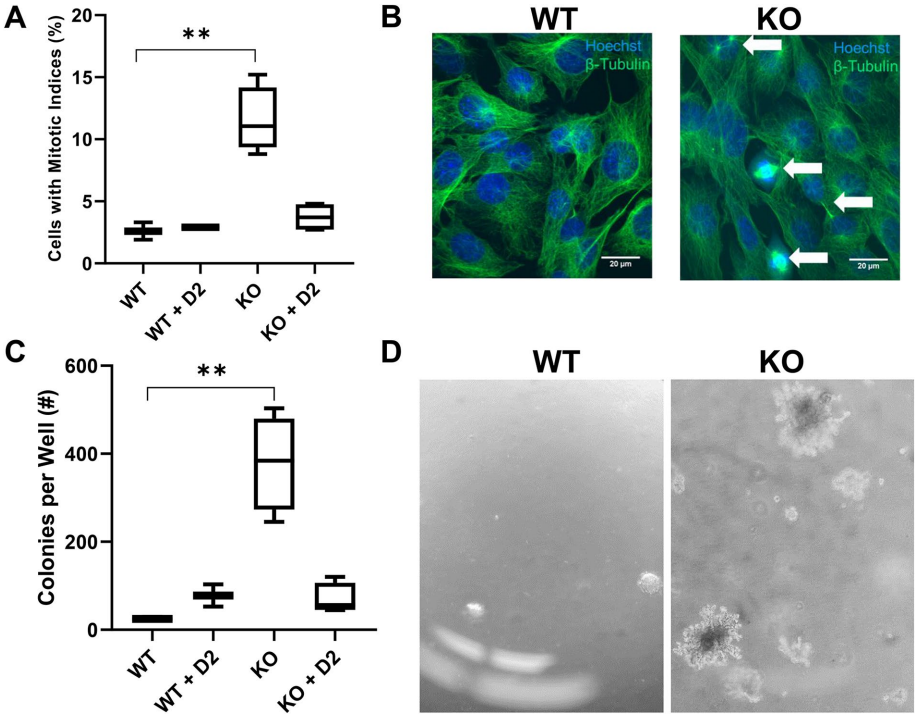

FIGURE 7: ELMOD2 nulls have higher mitotic index at high densities and increased anchorage-independent growth. (A) Cells were grown to high density, at or near confluence, before fixing and staining for α-tubulin and Hoechst, as described in *Materials and Methods*. Mitotic cells were quantified in duplicate (100 cells per replicate), and averages were graphed as box-and-whisker plots via GraphPad Prism. Statistical significance was assessed using one-way ANOVA; ** = $p < 0.01$. (B) Cells were prepared as described in panel A and imaged via confocal microscopy at 100× magnification, collecting *z*-stacks and generating a z-projection using FIJI software. White arrows indicate mitotic indices identified by DNA condensation and characteristic α-tubulin staining of mitotic spindles/midbodies. Scale bar = 20 μm. (C) The standard 12 lines were plated (20,000 cells/well) in triplicate, and colonies were scored after 30 d of growth in soft agar. This experiment was performed twice. Colonies were quantified using a stereomicroscope after fixing and staining with crystal violet (see *Materials and Methods*). Statistical significance was assessed using one-way ANOVA; ** = $p < 0.01$. (D) Colonies emerging after 30 d of culture, as described in panel C, were imaged by brightfield at 4× magnification. Images shown are representative of morphologies of colonies observed in WT and null lines.

again demonstrating the utility of such fast cycling mutants in ARF family members by avoiding irreversible or toxic effects of the GTPase defective mutants (Santy, 2002).

Because of the roles we found for ELMOD2 in microtubules, we did not want to exclude the possibility that at least part of the cell cycle defects could be a product of an ARL2-related pathway. Therefore, we also compared the effects of expressing the activating ARL2[V160A] or ARL3[L131A] mutants on multinucleation and supernumerary centrosomes. Neither appeared to have effects on these phenotypes in WT cells. Neither ARL2[V160A] nor ARF6-HA caused a significant change in the percentage of multinucleated cells in KO lines, but expression of ARL3[L131A] led to a small increase (from 22.0 to 27.5%; Figure 6G) in multinucleation in null lines that was statistically significant ($p < 0.05$). Thus, two different activating ARF6 mutants were highly specific, at least among this small subset of ARF family members, in reversing the increased nuclear number seen in ELMOD2 nulls.

Similar results were obtained upon scoring centrosome numbers (Figure 6G) in that both activating ARF6 mutants strongly reversed the supernumerary centrosome phenotype in KO lines ($p < 0.0001$). Like multinucleation, the ARF6[Q71L] caused increased centrosome numbers in WT cells, despite reversing the phenotype in nulls, while ARF6[T157A] had no effect on WT cells, yielding a cleaner and more readily interpretable result. Although small effects of activated ARL2 or ARL3 were seen in WT cells, they did not rise to the level of statistical significance ($p < 0.05$) and were well below that seen in ARF6[Q71L]-HA expressing cells. We saw no effects on centrosome numbers upon expression of ARF6-HA or ARL3[L131A]. Interestingly, expression of ARL2[V160A] yielded a partial reversal that was statistically significant ($p < 0.01$). Thus, only the two activating ARF6 mutants were found to strongly (essentially completely) reverse the increases in both the percentages of cells with multinucleation and supernumerary centrosomes; each appeared to be comparable in effectiveness.

These results demonstrate close functional links between ARF6 and ELMOD2 activities in MEFs with respect to their effects on nuclear and centrosome numbers. This stands in marked contrast to the specific functional ties between microtubule defects and ARL2 in ELMOD2 null lines, suggesting that ELMOD2 directs two different essential cellular functions through distinct GTPases.

ELMOD2 KO lines have lost contact inhibition and anchorage-independent growth

During the course of the investigations described above, we also noted two other phenotypes linked to ELMOD2 deletion. We include a brief description of them here, not to focus on additional mechanisms but simply to highlight the likelihood that ELMOD2 plays additional roles in the cell. We are still far from understanding all of its actions and how these functions may be integrated.

If cells were allowed to reach high cell densities, at or approaching confluence, we noted that ELMOD2 null lines displayed a higher percentage of cells undergoing cell division compared with wild-type lines (Figure 7, A and B). This higher mitotic index in confluent cultures is interpreted as evidence of the loss of contact inhibition. The standard 12 lines were scored in technical triplicate (counting 500 cells/line) and revealed that an average of 11.5% of KO lines were mitotic (ranging from 8.8% to 15.2%) while only 2.6% (range of 1.9–3.3%) of WT cells were dividing under these conditions (Figure 7, A and B). Expression of ELMOD2-myc resulted in reversal of this phenotype in KOs, as the average of the four lines dropped from 11.5% to 3.7%, while the WT lines showed no difference after transduction (2.6% vs. 2.9%). Thus, deletion of ELMOD2 in MEFs causes reduced contact inhibition, and this phenotype is rescued by expression of ELMOD2-myc.

Loss of contact inhibition is a common feature of cell transformation, so we next assessed another such property: the ability to grow in soft agar or anchorage-independent growth. We plated 2×10^4 cells in soft agar and monitored growth at 37°C over the course of

30 d, as described under *Materials and Methods*. The 12 standard lines were quantified in technical triplicate, with two biological replicates (Figure 7, C and D). While WT and ELMOD2-myc expressing WT cells had an average of 24 and 78 colonies, respectively, ELMOD2 nulls had >10-fold more colonies than WT (average of four lines = 379 colonies, range of 245–503 colonies) (Figure 7D). In addition, the few colonies seen in WT cultures were small (typically containing only a few cells), round, and symmetric. In contrast, the colonies from KO cultures were larger and often asymmetric in morphology. Thus, the loss of ELMOD2 in immortalized MEFs is accompanied by the acquisition of at least two phenotypes associated with cell transformation: loss of contact inhibition and gain of anchorage-independent growth. Neither of these phenotypes is predicted to be secondary to the effects described above on microtubules or cell division. Rather, these data are included simply to highlight the fact that additional cellular roles for ELMOD2 are evident. With each one, both the complexity and importance of this protein grow, as do the challenges in developing strong models for each action.

DISCUSSION

The generation of null MEF lines has revealed novel roles for the ARF GAP ELMOD2 in cytokinesis and microtubule stability and nucleation that are in addition to its previously documented roles in mitochondrial fusion (Newman *et al.*, 2017a; Schiavon *et al.*, 2019), in lipase recruitment to lipid droplets (Bouchoux *et al.*, 2011; Suzuki *et al.*, 2015), and in meiosis in oocytes (Zhou *et al.*, 2017). Our initial observations of cold sensitivity of cell morphology with loss of microtubules and multinucleation in ELMOD2 null cells were pursued through the use of multiple cell-based assays targeting different potential causes of these defects; our goal was to identify the sites and mechanisms of action. These assays have revealed a host of changes in cell functions resulting from the deletion of ELMOD2 that we believe can be traced back to fundamental defects in the recruitment of γ-TuRC to centrosomes, with consequent microtubule instability, and to the release of ARF6 from recycling endosomes resulting in downstream defects/failures in late cytokinesis or abscission (Figure 8). We also provide evidence that the defects observed in ELMOD2 nulls are linked to pathways involving (at least) two different ARF family GTPases: γ-TuRC recruitment with ARL2, and cytokinesis with ARF6. While pathways involving distinct GTPases have been demonstrated here, we cannot definitively rule out the possibility that defects in one impact the others. For example, altered microtubule stability or dynamics cannot be excluded from contributing to the delay in cell cycle. Similarly, we believe that other essential cell

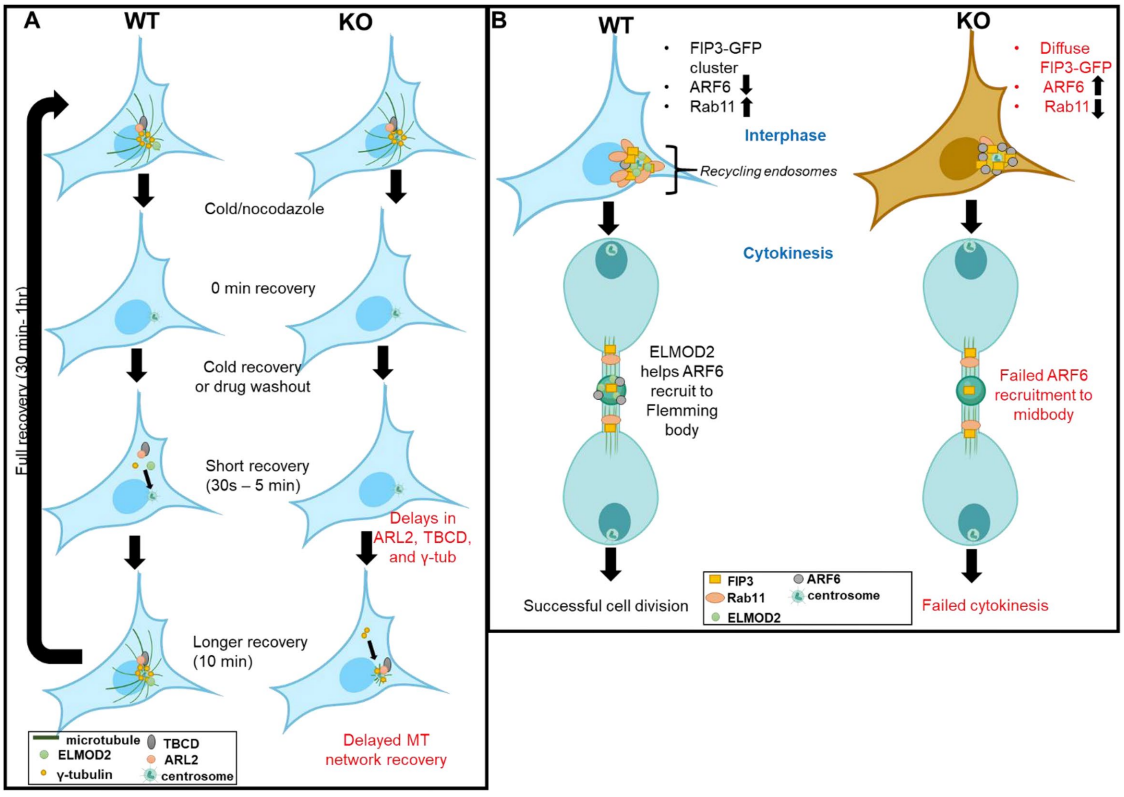

FIGURE 8: Model of ELMOD2's role in microtubules and cytokinesis. (A) We propose that the absence of ELMOD2 results in microtubule (cold and nocodazole) instability that is correlated with compromised retention and recruitment (during recovery) of γ-tubulin (and by extension γ-TuRC), ARL2, and TBCD at centrosomes. The higher retention of ARL2 and TBCD than γ-tubulin in all cells after cold treatment and effects of ELMOD2 overexpression (ELMOD2-myc) to increase ARL2 and TBCD retention in WT cells are suggestive of a role for ARL2 and TBCD in the recruitment of γ-tubulin to the PCM to allow centrosomal nucleation of microtubules. (B) We propose that ELMOD2 regulates cytokinesis through the ARF6/FIP3/Rab11 pathway(s). We propose that the absence of ELMOD2 results in altered binding of FIP3 (decreased), RAB11 (decreased), and ARF6 (increased) to endosomes, consistent with the previously proposed competition between ARF6 and RAB11 to bind FIP3. ARF6 fails to recruit to midbodies in the absence of ELMOD2, despite the presence of its binding partner MKLP1, contributing to delayed or failed cytokinesis/abscission. Whether these two effects are directly linked is currently unknown, but we speculate that the action of ELMOD2 as an ARF6 GAP at recycling endosomes may promote its dissociation at that site and may facilitate its recruitment to midbodies.

processes are likely to be affected by the loss of ELMOD2, as evidenced by the loss of contact inhibition and gain of ability to grow in soft agar. These two features of cell transformation were not further explored mechanistically, but we believe that they speak to the fundamental and far-reaching cellular roles of ELMOD2 and, by extension, the GTPases with which it acts.

We interpret cold sensitivity and nocodazole supersensitivity of the microtubule network in the ELMOD2 nulls as most consistent with a decrease in the overall stability of the microtubule network. The regulation of microtubules and their dynamics is incredibly complex but, on the basis of our data, we predict that ELMOD2 acts with ARL2 at centrosomes at least in part to promote the recruitment of the γ-TuRC. We cannot exclude other possibilities for how ELMOD2 may be working with ARL2, as ARL2 is also a critical player in regulating the assembly of αβ-tubulin heterodimers through the tubulin folding pathway (Bhamidipati *et al.*, 2000; Radcliffe *et al.*, 2000; Beghin *et al.*, 2007; Tian *et al.*, 2010; Nithianantham *et al.*, 2015; Francis *et al.*, 2016, 2017a,b). However, our data reveal delays in γ-tubulin, ARL2, and TBCD recruitment during recovery from cold, leading us to propose a model (Figure 8) in which ELMOD2 regulates ARL2 activity and perhaps less directly TBCD and γ-TuRC. Furthermore, the decreased aster size and number of microtubules emanating from asters suggest that even when γ-tubulin does recruit, there is still a delay in microtubule growth (Figures 1 and 2). Further studies into the ordering of recruitment of these components to centrosomes and the mechanisms by which they work together to regulate microtubule nucleation at centrosomes is warranted and predicted to reveal further insights into the actions of each of these proteins.

With our earlier focus on the role of ELMOD2 inside mitochondria, we used fixation and permeabilization methods optimal for that organelle and missed the fact that ELMOD2 also localizes to centrosomes, or more specifically the PCM. After switching to the most common fixative for looking at centrosomal proteins (cold methanol), we were able to demonstrate the specific localization of ELMOD2 at that site, where we had previously shown ARL2 and TBCD to be present (Zhou *et al.*, 2006; Cunningham and Kahn, 2008). The greater cold induced release of all of these, along with γ-TuRC, and delays in their return in ELMOD2 null cells (compared with WT) provide correlative evidence of them acting together. Work from our and other labs have demonstrated direct interactions between ARL2 and ELMOD2 and between ARL2, TBCD, and β-tubulin, though not previously at centrosomes. The finding that rescue of the ELMOD2 loss requires its GAP activity supports the conclusion that it is acting through ARL2 in this pathway. The fact that fast cycling ARL2 (which is still sensitive to GAP action) rescues the cold sensitivity is consistent with ELMOD2 regulating the cycling, and thus the half-life, of activated ARL2 at centrosomes. Clearly more work is needed to provide the molecular mechanisms by which ARL2 and ELMOD2 are acting at the PCM to influence γ-TuRC recruitment and microtubule growth/stability, but these initial findings reveal novel roles for each that also will need to be dissected from their other essential cellular roles.

Placing a population of ELMOD2 at centrosomes could also potentially explain the effects of its deletion on the recruitment of FIP3, RAB11, and ARF6 to recycling endosomes. Although we did not detect ELMOD2 staining in the endosome clusters that are defined by FIP3-GFP, their close proximity to centrosomes may suggest a functional link. Deletion of ELMOD2 caused defects that can be attributed to either a delay or a failure in cell division late in the process, perhaps immediately preceding abscission. The delay is most evident from the extended stalling observed in time required to complete cytokinesis after removal of the CDK1 inhibitor (Figure 4B) and the large increase in the percentage of cells having midbodies (Figure 4C). Multinucleation, supernumerary centrosomes, and polyploidy (Figure 3) typically result from failure in cytokinesis. In efforts to identify a specific lesion present in cells lacking ELMOD2, we used immunofluorescence to monitor the localization of multiple markers of cytokinesis that are recruited to specific sites (recycling endosomes, midbodies, ICB, or Flemming body) at precise times during cytokinesis. Most of these were unchanged between WT and ELMOD2 null cells. In contrast, staining of ARF6 is lost at the Flemming body in ELMOD2 KO cells. MKLP1 binds to activated ARFs and recruits ARF6 to the Flemming body (Boman *et al.*, 1999; Van Valkenburgh *et al.*, 2001; Makyio *et al.*, 2012). ARF6 is required for completion of cytokinesis (Schweitzer and D'Souza-Schorey, 2002, 2005; Schweitzer *et al.*, 2011). MKLP1 is still present in null cells while ARF6 is not. We propose (Figure 8) that the lack of ELMOD2 causes a defect in the translocation of ARF6 to that site, with consequent increased failures in abscission. This might result from a defect in the spatial and/or temporal activation of ARF6 that is required for its functionality at that site- for example, a role for ELMOD2 in recruiting an ARF6 guanine nucleotide exchange factor (GEF) in a GTPase network (Mizuno-Yamasaki *et al.*, 2012). This is also consistent with the finding that the fast cycling, activated ARF6 reverses this defect upon expression in null cells (Figure 6, G and H). The mechanism by which ELMOD2 plays a role in ARF6 recruitment to the midbody (and how ELMOD2 itself recruits to the midbody) requires further exploration. Despite the lack of specific ELMOD2 staining at recycling endosomes, we cannot exclude the possibility that it also can be recruited to recycling endosomes. As suggested above, the close physical proximity of these recycling endosomes to the PCM might allow for transient protein interactions that do not survive fixation.

While RAB11 staining was reduced, we saw the opposite changes in ARF6 staining at FIP3–positive recycling endosomes in response to deletion of ELMOD2; ARF6 was strongly increased (Figure 6). The order and specific interactions involved in recruitment of FIP3, RAB11, and ARF6 to recycling endosomes are unresolved, though FIP3 can bind to RAB11 and ARF6 and potentially even at the same time, based on in vitro binding assays (Fielding *et al.*, 2005; Shiba *et al.*, 2006; Schonteich *et al.*, 2007; Takahashi *et al.*, 2011). Our data support a role for ELMOD2 in this process. Fielding *et al.* (2005) also showed staining of ARF6 at the ICB but not at the Flemming body. In contrast, we found ARF6 at the Flemming body but not evident at the ICB. Much (though not all) of the evidence that ARF6 localizes to the ICB in this earlier study was obtained using ARF6[Q71L] and thus may result in trapping of the mutant that is incapable of cycling between active and inactive conformations. Expression of FIP3-GFP in WT cells allows visualization of the pericentrosomal pool of recycling endosomes, and that stains strongly for RAB11 but not for ARF6 (Figure 6). ELMOD2 deletion hampers the recruitment of FIP3 to these endosome clusters, causes a severe loss of RAB11 staining there, and is accompanied by large increases in ARF6. However, when FIP3 staining is diffuse and FIP3-GFP–positive endosomes are no longer evident, ARF6 also does not localize to endosomal clusters. Thus, we interpret these findings as consistent with a model in which ARF6 is recruited to recycling endosomes by FIP3 and competes for this binding with RAB11. The presence of ELMOD2 in WT cells at or nearby this site may result in rapid inactivation of ARF6 and favor the binding of RAB11 to FIP3.

Because the binding of RAB11 or ARF6 to FIP3 is dependent on activation (GTP binding), there are two likely ways that ELMOD2 might increase RAB11 and decrease ARF6 at recycling endosomes:

it could recruit a RAB11 GEF or act as an ARF6 GAP. Given the established activity of ELMOD2 as an ARF/ARL GAP, we clearly favor the latter of these and conclude that the deletion of ELMOD2 causes ARF6 to accumulate on recycling endosome by decreasing the cell's ability to inactivate the GTPase there. That increase in ARF6 competes effectively with RAB11 for the binding to FIP3. It is not clear whether ELMOD2 might have some additional effect resulting in the loss in FIP3 recruitment to recycling endosomes. It could be the case that FIP3 is more stably bound at this site when complexed with RAB11 than to ARF6. The strong and specific effects of activated ARF6 to reverse the multinucleation and supernumerary centrosome phenotypes (Figure 6) in ELMOD2 are consistent with those phenotypes being linked.

Because of the central role of microtubules in the mitotic spindle and cell division, we expected to find close ties between the cytokinesis failure and the changes in microtubules observed, but instead we interpret our findings as evidence of two different roles for ELMOD2 in cells and acting with two different GTPases. While ARF6 is capable of influencing actin at the cell surface (D'Souza-Schorey and Chavrier, 2006), there are no published links between ARF6 and microtubules/tubulins. ARL2, though, has well documented roles in assembly of the αβ-tubulin heterodimer and in altering microtubule networks when overactivated- for example, upon expression of the dominant activated mutant ARL2[Q70L] (Zhou *et al.*, 2006). Indeed, decreased stability of microtubules and increased sensitivity to microtubule destabilizing drugs were among the first phenotypes found for mutants of ARL2 in multiple genetic model systems (Hoyt *et al.*, 1990; Stearns *et al.*, 1990; Antoshechkin and Han, 2002; Steinborn *et al.*, 2002). The fact that we first purified ELMOD2 as a GAP for ARL2 also prompted us to focus on this GTPase as likely to be playing a central role in the microtubule defects seen in ELMOD2 null cells. The specificity of rescue by activated ARL2 but not ARL3 or ARF6 further supports it acting with ARL2 here. We currently model the actions of ELMOD2 in cells, specifically in microtubule stability and cytokinesis, as acting in distinct pathways that use distinct ARF family GTPases. Consistent with this, we observed no clear evidence of a defect in mitotic spindles or midbody bridge morphology in the nulls, based on α-tubulin or γ-tubulin staining, suggesting that any cytokinesis defects we observe are not an overt consequence of ELMOD2-related microtubule instability. Our results are similar to, though different, from those of Zhou *et al.* (2017) in which they found aneuploidy in mouse oocytes knocked down for ELMOD2 but with "severe abnormalities in spindle organization" that we did not observe in null cells. Furthermore, fast cycling ARL2 only partially rescued cell cycle–related defects, and active ARF6 did not rescue the microtubule defects. Thus, despite our original conjecture that the microtubule and cell cycle–related phenotypes may result from a single lesion arising from the absence of ELMOD2, our data clearly argue for at least two distinct lesions, each of which can be mitigated through increased activation of distinct GTPases.

This study also describes for the first time the use of multiple "fast cycling" mutants for ARF family GTPases, first described by Lorraine Santy for ARF6 (Santy, 2002) and later employed by others for multiple family members (D'Souza *et al.*, 2020; Moravec *et al.*, 2012). This and structural studies have confirmed the conserved function of homologous residues in the GTP binding pocket in making direct contacts with the guanine base. Mutations that decrease this interaction result in weakened affinity for GDP and thus increase the rate-limiting step in GTPase activation: release of GDP. These mutants provide an important adjunct to the common use of glutamine mutants (e.g., Q70L in ARL2) that are also activating in cells. The stronger Q to L mutants may be so strong as to generate phenotypes that obscure or make analyses of other actions unfeasible. This is particularly problematic when studying a regulator of the GTPase that acts at multiple sites and with multiple GTPases. We believe that this is the case with ARL2[Q70L], further demonstrating the value of fast cycling mutants.

Similarly novel, and perhaps confusing, is the use of activated GTPase mutants to rescue the deletion of a GAP. Clearly, in this use the "rescuing GTPase" cannot be acting as the substrate for the deleted GAP (ELMOD2). In such a case where a GEF activates the GTPase and the GAP silences that activity, one should not see "rescue" by further increasing the activity of the GTPase in question. Instead, we are speculating that rescue is achieved in one of two, not mutually exclusive, ways. Our preferred hypothesis is that the pathways in question are acting as GTPase networks such as those described by Mizuno-Yamasaki *et al.* (2012). In this scenario, an activated GTPase recruits its own GAP and effectors, and one of those effectors also possesses GEF activity for another GTPase acting downstream of the first. Thus, if activated ARF6 or ARL2 rescues a defect observed upon deletion of ELMOD2, we are not concluding in either case that ELMOD2 normally acts as a GAP on the GTPase in that pathway and location. Rather, we propose that those GTPases share a common pathway with ELMOD2 but instead act downstream. Yet, we cannot exclude the possibility that the same GTPase *also* acts upstream of ELMOD2. For example, a number of the ARF family GTPases that ELMOD2 acts on in vitro (including ARF1, ARF3, and ARF6) have been shown previously to regulate aspects of cytokinesis and to localize to key sites in this process (e.g., centrosomes, cleavage furrows, and midbodies [D'Souza-Schorey and Chavrier, 2006; Hanai *et al.*, 2016]). Further research should be devoted to finding which GTPase(s) ELMOD2 acts with directly to mediate these functions and identifying the mechanism by which it regulates both cytokinesis and γ-TuRC recruitment. The other possibility is that the cell system under study involves parallel pathways, only one of which involves ELMOD2 and the other is under regulation by the rescuing, activated GTPase. Of course, these are not mutually exclusive, pointing to the potential for complexities and the amount of work left to do in deconvoluting mechanisms of regulation of these essential cell processes (Sztul *et al.*, 2019).

Two other issues that we considered as having the potential to influence the interpretation of our data are the existence of two other ELMOD family members and three other ELMO proteins (East *et al.*, 2012). Parallel studies using CRISPR-Cas9 generated deletions of ELMOD1 and ELMOD3 in MEFs have revealed none of the same phenotypes described here for ELMOD2, though they, too, are implicated in multiple processes (unpublished data). Though quantification of these three proteins is difficult because of their low abundance, we used real-time quantitative reverse transcription PCR in that study and found no evidence of up-regulation of other ELMOD family members in response to deletion of any one. Thus, we do not believe that the results described here are explained by changes in activities of ELMOD1 or ELMOD3, though of course we cannot exclude some level of functional redundancy or actions of either protein in microtubule dynamics or cell division. In addition, ELMO proteins share the ELMO domain with the ELMODs and are found in cells bound to DOCK proteins (e.g., DOCK180) that possess RAC/RHO GEF activity (Gumienny *et al.*, 2001; Brugnera *et al.*, 2002; Lu *et al.*, 2004). Furthermore, ARF6 and its GEF ARNO (aka cytohesin 2) activate RAC via ELMO1/DOCK180 (Santy *et al.*, 2005), influencing actin dynamics and cell motility. To date, there have been no studies showing functional redundancies between ELMOD and ELMO proteins. It is worth noting the existence of each, though, particularly as they share some common pathway components (e.g., ARF6).

In summary, this work provides evidence for essential roles for ELMOD2 in both cytokinesis and microtubule dynamics. To our knowledge, this is the first evidence of one ARF GAP acting in cells to influence pathways involving both ARF(s) and ARL(s). The previously described (Ivanova *et al.*, 2014) biochemical promiscuity of ELMODs as GAPs makes them prone to even greater complexity in serving as signaling hubs to bring together disparate, but highly regulated, processes. Future studies into the mechanisms by which ELMOD2 modulates cytokinesis and microtubule stability should provide further insights into those processes as well as whether and how apparently diverse pathways may communicate with one another. When these results are considered together with those demonstrating roles for ELMOD2 in mitochondrial fusion (Newman *et al.*, 2017a; Schiavon *et al.*, 2019), in fat metabolism at lipid droplets (Suzuki *et al.*, 2015), and in anchorage-independent growth (Figure 7), there is clearly a need for further study of these pathways and their potential for interconnections. Together, these results significantly extend the functions and locations at which ELMOD2 acts in cells, working with multiple GTPases to mediate these processes.

MATERIALS AND METHODS

Reagents, antibodies, plasmids

The antibodies raised against the following proteins were purchased: α-tubulin (Sigma; T9026), β-tubulin (Sigma; T4026), α-tubulin (Millipore-Sigma; rat monoclonal; MAB1864), γ-tubulin (Sigma; T6557), γ-tubulin (Abcam; ab11317), centrin (Sigma; 04-1624), RAB11 (Transduction Laboratories; R56320), myc (Invitrogen; R950-25), HA (Covance; MMS-101P), and acetylated tubulin (Sigma; T6793-2ML). The following rabbit polyclonal antibodies were generated against their respective human proteins and have been described previously: ARL1 (Van Valkenburgh *et al.*, 2001), ARL2 (Sharer and Kahn, 1999; Sharer *et al.*, 2002), ARL3 (Cavenagh *et al.*, 1994), BART (Sharer *et al.*, 2002), TBCD (Francis *et al.*, 2017b), and ELMOD2 (Newman *et al.*, 2014). RHOA (Abcam; ab54835) and ARF 1D9 monoclonal (Affinity Bioreagents; MA3-060 [Cavenagh *et al.*, 1996]) antibodies were obtained commercially. We are grateful for the generous gifts of other antibodies: ARF6 polyclonal antibody from Jim Casanova (University of Virginia), rabbit polyclonal antibodies directed against FIP1 and FIP5 from Rytis Prekeris (University of Colorado), polyclonal sheep-anti-FIP3 from Jim Goldenring (Vanderbilt University), and mouse monoclonal antibodies against MKLP1 from Ryoko Kuriyama (University of Minnesota) (Kuriyama *et al.*, 1994).

The CRISPR-Cas9 system used for transfection into MEFs was obtained commercially from Addgene (pSpCas9(BB)-2A-Puro (PX459) V2.0 (#62988)). Plasmids directing expression of human ARL2, ARL2[Q70L], ELMOD2-myc, ELMOD2-HA, or ELMOD2[R167K]-myc/his in pcDNA3.1 were described previously (Zhou et al., 2006; Bowzard *et al.*, 2007; East *et al.*, 2012). The following plasmids were gifted to us by Rytis Prekeris: FIP1-GFP and FIP5-GFP. Jim Goldenring gifted us with FIP3-GFP (Hickson *et al.*, 2003). Jim Casanova provided us with plasmids used for transient expression of ARF6-HA, ARF6[Q71L]-HA, or ARF6[T157A]-HA. All fast cycling point mutants were generated in pcDNA3.1 vectors using site-directed mutagenesis. The following reagents were purchased: nocodazole (VWR; 102515-934), thymidine (Sigma; T1895-10G), RO-3306 CDK1 inhibitor (Sigma; SML0569-25MG), and oleic acid (Sigma; O1383-5G).

Cell culture

Cells used in this study were grown in DMEM supplemented with 10% fetal bovine serum (FBS) (Atlanta Biologicals; S11150) and 2 mM glutamine at 37°C, 5% CO_2. WT MEFs were obtained from the American Type Culture Collection (ATCC) (CRL-2991). Antibiotics are not used in routine cell culture, and cells are regularly checked for mycoplasma contamination. All phenotypes described were monitored in MEF lines maintained below passage 10, to avoid the potential selection against cell cycle defects observed in ELMOD2 nulls. Cells with different genotypes were all maintained with careful attention to ensure the same feeding, passaging, and plating density, though densities at plating may differ between assays. For all experiments described below, we consider replicates of individual lines repeated on different days as technical replicates, and the averages of technical replicates performed for each line are considered biological replicates.

Generation of CRISPR null lines

WT (parental; ATCC CRL-2991) immortalized MEFs served as the parental population for the ELMOD2 KO lines generated via CRISPR-Cas9. Benchling software (www.benchling.com/academic/) was used to design four 20 nt guides. To facilitate expression from the U6 promoter, a "G" was substituted for the first nucleotide for each guide RNA. Overlapping primers with *Bbs*I overhangs at the 5′-end were purchased from IDT based on the following templates: 5′-CACC$(N)_{20}$-3′ and 5′-AAAC$(NR)_{20}$-3′, where $(N)_{20}$ and $(NR)_{20}$ refer to the 20 nt protospacer sequence and its reverse complement, respectively. The two complimentary oligos were annealed and cloned into pSpCas9(BB)-2A-Puro (PX459) V2.0 vector (Addgene) at the *Bbs*I sites. These guides were targeted close to the N-terminus of the protein to optimize the likelihood of null alleles that yield little of the ELMOD2 protein. Our goal was to generate at least two different clones from at least two different guides, each with frameshifting mutations on both alleles.

Low-passage MEFs were grown to 90% confluence in six-well dishes, transfected with a 1:3 ratio of DNA (guide RNA plasmids) to Lipofectamine 2000 for 4 h in OptiMEM, and then replated onto 10 cm plates for growth overnight. Puromycin (3 μg/ml; Sigma #P8833) was added the next day and maintained for 4 d to enrich for transfected cells. Individual clones were isolated via limited dilution in 96-well plates, followed by expansion, cryopreservation, and sequencing of genomic DNA around the target site.

To ensure that any phenotypes we identified were solely the consequence of a loss of ELMOD2, we used the following controls: 1) generated at least two different clones from at least two different guides and 2) performed rescue experiments by expressing ELMOD2-myc using lentivirus transduction into null cells, as well as WT cells, which served as further controls. All phenotypes described here were present in all 10 null lines, though varied in magnitude when scored. Four of the 10 null lines were chosen at random for more detailed studies and quantification.

Transfection of MEFs

For all other transfections of WT or ELMOD2 null MEFs, polyethylenimine (PEI) transfection was used instead of Lipofectamine as it proved to be less toxic and yielded higher transfection efficiencies. Cells were transfected with a 1:3 ratio of DNA to PEI for 24 h in medium containing 2% serum before being replated onto coverslips. In most cases, 4 μg of DNA, 12 μg of PEI, and 100 μl of serum-free medium per reaction were combined in an Eppendorf tube, vortexed, and allowed to incubate for 20 min. The DNA/PEI mixture was added dropwise to each respective well, and samples were returned to 37°C to incubate overnight. The next day, cells were replated as needed for different experiments.

Lentiviral transduction

A lentivirus directing expression of mouse ELMOD2-myc was generated by Emory's Viral Vector Core, using the pFUGW vector into which the mouse ELMOD2-myc open reading frame was engineered at the *Eco*RI and *Bam*HI sites. About 10,000 cells were plated into wells of a 24-well plate and were treated with lentivirus 2 h later. Medium was replaced after 48 h. The efficacy of lentiviral transduction was checked using immunocytochemistry, staining for myc expression. Transduction efficiency was estimated between 70 and 90% depending on the line. For all the following rescue experiments, all cells were counted under the assumption that the majority of the cells scored express ELMOD2-myc. This may account for the heterogeneity in phenotypic rescue and may also result in underestimates of the magnitude of the rescue achieved.

Lipid droplet staining

Cells were plated onto Matrigel-coated coverslips and the next day were treated with or without oleic acid (30 μM at 37°C for 24 h; vortexed in solution with DMEM + 10% FBS + 1% bovine serum albumin [BSA] prior to addition to cells) to increase lipid droplet accumulation. Cells were fixed with 4% PFA for 15 min at 37°C and permeabilized with 0.1% Triton X-100 for 15 min. To visualize lipid droplets, cells were stained for 30 min with a 1:100 dilution of BODIPY 493/502 (Invitrogen; D3922) (0.5 mg/ml stock) in phosphate-buffered saline (PBS). Brightfield (20× magnification) and widefield fluorescence microscopy (100× magnification) were used to assess lipid droplet numbers and sizes by visual inspection.

Scoring mitotic cells and high cell density

Cells were grown to high confluence (>90%) on glass coverslips and fixed with 4% PFA in PBS (137 mM NaCl, 2.7 mM KCl, 10 mM Na_2HPO_4, 1.8 mM KH_2PO_4, pH 7.4). Cells were permeabilized with 0.1% Triton X-100, blocked with 1% BSA in PBS, and stained with Hoechst (10 mg/ml stock in water; diluted 1:5000 in PBS and stained for 4 min), tubulin, and γ-tubulin to track mitotic indices. Five hundred cells were scored per replicate. Cells were binned based on the following features: DNA condensation at prophase, aligning of DNA at the metaphase plate and mitotic spindle staining during metaphase, separation of condensed DNA without cleavage furrow formation during anaphase, cleavage furrow formation during telophase, and midbody staining and DNA decondensation during late cytokinesis.

Growth in soft agar

Anchorage-independent growth, or the ability to grow in soft agar, was assessed as previously described (Borowicz *et al.*, 2014). Briefly, 20,000 cells were plated in individual wells of a six-well dish in soft (1 ml, 0.7%) agar over a base of 1 ml 1.0% agar in DMEM with 10% FBS. Cells were monitored for 30 d, with the addition of fresh medium dropwise every few days to prevent dehydration. Cells were stained with 0.5 ml 0.005% crystal violet in methanol for 2 h at room temperature before being rinsed three times with water. Colonies that are positive for crystal violet and at least three cells in diameter (≥~10 cells) were scored using brightfield microscopy.

Nocodazole sensitivity

Cells were treated with a range of concentrations of nocodazole (0–100 ng/μl) for 2 h. Cells were then fixed with ice-cold methanol for 5 min at –20°C. They were then blocked and stained for α-tubulin to identify microtubule networks and γ-tubulin to identify centrosomes. Cells were visualized via widefield microscopy and binned by visual inspection based on whether they had intact versus defective microtubule networks. microtubule networks were defined as "defective" if they had either an obvious decrease or a complete loss of microtubule network compared with that seen in WT cells (see Supplemental Figure S4, for example).

Cold sensitivity

Cold sensitivity was determined by removing cells from the incubator and exposing them to room temperature or putting them on ice (as indicated in the text) for a defined period of time ranging between 0 and 30 min. Immediately after, the cells were fixed with prewarmed (37°C) 4% PFA and permeabilized with 0.1% Triton X-100. Samples were stained for α-tubulin to denote microtubule networks and γ-tubulin to identify centrosomes. Like the nocodazole sensitivity assay described above, microtubule network density was assessed by visual inspection (see Supplemental Figure S4, for example).

For cold sensitivity recovery experiments, cells were removed from the incubator and incubated on ice for 30 min. Afterward, cells were returned to the incubator at 37°C and allowed to recover for a range of time points extending from 0 min to 1 h recovery. Cells were fixed either with 4% PFA and permeabilized with 0.1% Triton X-100 to look at microtubules and γ-tubulin or with ice-cold methanol for 5 min to visualize centrin at centrioles. The latter condition was also used to visualize ARL2 and TBCD at centrosomes. Cells were visualized with either widefield microscopy for basic scoring or confocal microscopy to generate *z*-projections to score microtubules at asters.

Scoring microtubules at centrosomes after cold recovery

Cells were treated as described above for cold sensitivity recovery, incubating the cells for the specified time points at 37°C to allow partial regrowth of microtubules. Cells were fixed with 4% PFA for 15 min at 37°C, permeabilized with 0.1% Triton X-100 for 10 min, and stained for γ-tubulin to look at recovery at centrosomes and for α-tubulin to look at microtubule formation at asters. Cells were imaged using confocal microscopy (as described below) taking *z*-projections with 0.37 μm steps. These *z*-projections were processed using FIJI software to look at individual slices of cells and to visualize microtubules emanating from centrosomes. Microtubules were scored if 1) one of the ends of the microtubule could be seen extending from a γ-tubulin–positive centrosome, and 2) if the tubule was at least 0.5 μm long, as determined using FIJI. The number of microtubules emanating from that centrosome were scored in each slice, and the slice with the highest number of microtubules was used to score that aster. After analyzing cells from multiple replicates, a total of at least 38 asters were scored per line.

Aster formation assay

The extent of aster formation as a function of time after removal of nocodazole was used as a way to measure the rate of growth of new microtubules at centrosomes, as previously described (Sankaran *et al.*, 2005; Tulu *et al.*, 2006; Zhou *et al.*, 2006; Cunningham and Kahn, 2008). Microtubules were found to be eliminated, with minimal cellular toxicity, by treatment with 50 ng/μl nocodazole for 2 h at 37°C. The drug was then removed, cells were washed once, and fresh prewarmed medium was added. Cells were fixed at 0, 0.5, 1, 2, 5, 7, and 10 min after release from nocodazole using 4% PFA and 0.1% Triton X-100 permeabilization. Cells were stained for α-tubulin and γ-tubulin, as described above. The size of asters as well as the morphology of the growing microtubule network were then assessed. To quantify aster size, the diameter of individual asters was measured using FIJI imaging software's measuring tool. For each aster, the largest diameter was determined and then tabulated. At

least 50 asters were quantified per line per replicate, and the average aster diameter was determined per line (see Supplemental Figure S5, for example).

Scoring of cell phenotypes

To score numbers of nuclei, cells were plated onto glass coverslips at 50–60% confluence to facilitate scoring of individual cells. The next day, cells were fixed with 37°C 4% PFA in PBS for 15 min at room temperature. Cells were permeabilized for 10 min with 0.1% Triton X-100 in PBS and blocked for 1 h with PBS with 1% BSA. Primary antibodies were incubated at least 1 h to overnight. The next day, cells were washed 4× with PBS and incubated with secondary antibody in PBS with 1% BSA. Cells were washed twice with PBS, stained with 1:5000 Hoechst 33342 for 4 min, and washed twice again with PBS before being mounted onto slides with 1:9 solution of PPD (*p*-phenylenediamine dihydrochloride; ACROS Organics; 624-18-0) in MOWIOL 4-88 Reagent (CALBIOCHEM; 475904). Cells were scored in triplicate for each of the 21 lines studied, 100 cells per replicate.

Scoring of centrosomes was performed using immunofluorescence, after methanol fixation, using two centrosomal markers (centrin and γ-tubulin). At least 100 cells were scored per condition per line, and this experiment was repeated at least three times.

Live cell imaging

Cells were plated on eight-well Ibidi glass-bottom slides (Ibidi #80827) at medium density, and 24 h later medium was replaced with imaging medium (phenol red-free DMEM with 25 mM HEPES, 10% FBS [Invitrogen #21063]). Cell cycle was tracked with phase-contrast illumination at 40× magnification (0.60 NA) using a BioTek Lionheart FX widefield microscope. Several fields of cells were collected over a 24 h time course at 37°C, 5% CO_2 every 10 min. *Z*-projections were generated to detect all cells, including those detaching from the plate during cell division. To track stages of cell division, different aspects of cell morphology were noted, including cell rounding (indicative of prophase/metaphase), cell elongation and cleavage furrow formation (anaphase proceeding into telophase), cleavage furrow narrowing into midbodies (cytokinesis), and cells splitting apart during abscission.

Scoring of cell cycling and synchronization

Cells were grown on Matrigel-coated coverslips to ~50% density and treated with the CDK1 inhibitor (RO-3306; 7.5 μg/ml) in DMEM with 10% FBS. After 18 h, cells were rinsed once and grown in fresh medium, taking time points after release from drug every 10 min for 2 h. Cells were fixed in 4% PFA in PBS for 15 min at room temperature, rinsed three times in PBS, and then permeabilized with 0.1% Triton X-100 in PBS for 10 min, followed by blocking with 1% BSA in PBS for 1 h. The cells were stained with antibodies directed against α-tubulin (to mark mitotic spindles and midbodies) and γ-tubulin (to mark centrosome migration throughout the cell cycle and midbodies), and Hoechst 3052 (diluted 1:5000 in PBS from 5 mM stock). Cells were scored as mitotic if DNA was condensed and aligned along the midplate and a mitotic spindle was evident, or if nuclear envelopes had formed and the midbody was evident from the α-tubulin staining. We use the term "mitotic indices" to indicate cells bearing traits of anywhere from prophase to late cytokinesis, for example, DNA condensation, mitotic spindle formation, cleavage furrowing/ingression, and midbody formation.

Analyzing DNA content

Cell synchronization was performed using a double thymidine block followed by nocodazole using the following protocol: cells at ~50% confluence were treated for 16 h in 2 mM thymidine, then allowed to recover for 8 h in drug-free medium after 3× washes with PBS, another 16 h thymidine block, followed by a 5 h recovery in drug-free medium after 3× washes in PBS, and then 9 h in medium containing nocodazole (20 ng/ml). Immediately after nocodazole synchronization, cells were prepared for analysis by flow cytometry by collecting cells, washing them with ice-cold PBS, and fixing them with ice-cold 70% ethanol in PBS. Note that all cells were collected and fixed at this stage to ensure a full representation of the cell population. Immediately prior to cytometry, cells were washed twice with phosphate citrate buffer (0.1 M citric acid in PBS, pH 7.8), treated with RNase (100 μg/ml; Sigma; R5125), and stained with propidium iodide (50 μg/ml; Sigma; P4170) to measure DNA content. The voltage was set based on WT cells for each run, centering the G1 peak at 50 K. The same settings were applied to all subsequent samples run that day, to ensure that we accurately tracked 2N, 4N, and >4N peaks. Data were plotted using FloJo software.

Microscopy

For all immunocytochemistry experiments, Matrigel (BD Bioscience)-coated 18 mm glass coverslips (#1.5; Fisher Scientific; 12-545-81) were used. Imaging was performed on a confocal microscope (Olympus FV1000 and Olympus Fluoview v1.7 software; 100× magnification [1.45 NA, oil]; 405, 488, and 543 laser lines used, 0.37 μm step size for *z*-stacks) and a widefield microscope (Olympus IX81 and Slidebook software; 100× magnification [UPlanFl, 1.30 NA oil], as indicated in the provided figures. Images were processed (and analyzed, in the case of aster formation assays) using FIJI imaging software. For all data appearing in any one figure, the same acquisition, brightness, contrast, cropping, and other processing settings were used across the experimental test group to ensure the accuracy of comparisons.

Reproducibility/statistics

All experiments performed in this study were scored at least in duplicate and performed at least in triplicate. Unless otherwise stated, at least 100 cells were scored per sample. Error bars presented in the graphs indicate SEM, and box-and-whisker plots indicate the range of the data along with the median and upper/lower quartiles. One-way or two-way analysis of variance (ANOVA) tests were used to determine whether there were significant differences between test groups. The number of stars indicates the level of statistical significance: $*p < 0.05$; $**p < 0.01$; $***p < 0.0001$. For all experiments shown, we treated individual replicates (separate samples from experiments performed on separate days) of each individual line as technical replicates. We consider the individual lines as biological replicates. Therefore, if we report that a sample has an $N = 4$, this indicates that four different lines were scored in duplicate, and the averages of those duplicates are presented in the graphs.

ACKNOWLEDGMENTS

This work was supported by National Institutes of Health Grants R35GM122568 to R.A.K. and 1F31CA236493-02 to R.E.T. We thank colleagues for their generous sharing of key reagents: Jim Casanova (University of Virginia; ARF6 antibody and ARF6 mutant plasmids), Jim Goldenring (Vanderbilt University; FIP3 plasmid and antibody), and Ryoko Kuriyama (University of Minnesota; MKLP1 antibodies). This research was supported in part by the Emory University Integrated Cellular Imaging (ICI) Microscopy Core and Emory Viral Vector Core of the Emory Neuroscience NINDS Core Facilities Grant 5P30NS055077. We thank the Emory Biochemistry Department and

Laney Graduate School for all the support and shared resources provided.

REFERENCES

Adari H, Lowy DR, Willumsen BM, Der CJ, McCormick F (1988). Guanosine triphosphatase activating protein (GAP) interacts with the p21 ras effector binding domain. Science 240, 518–521.

Agromayor M, Martin-Serrano J (2013). Knowing when to cut and run: mechanisms that control cytokinetic abscission. Trends Cell Biol 23, 433–441.

Antoshechkin I, Han M (2002). The C. elegans evl-20 gene is a homolog of the small GTPase ARL2 and regulates cytoskeleton dynamics during cytokinesis and morphogenesis. Dev Cell 2, 579–591.

Aspenstrom P (2018). Fast-cycling Rho GTPases. Small GTPases 11, 248–255.

Beghin A, Honore S, Messana C, Matera EL, Aim J, Burlinchon S, Braguer D, Dumontet C (2007). ADP ribosylation factor like 2 (Arl2) protein influences microtubule dynamics in breast cancer cells. Exp Cell Res 313, 473–485.

Bhamidipati A, Lewis SA, Cowan NJ (2000). ADP ribosylation factor-like protein 2 (Arl2) regulates the interaction of tubulin-folding cofactor D with native tubulin. J Cell Biol 149, 1087–1096.

Boman AL, Kuai J, Zhu X, Chen J, Kuriyama R, Kahn RA (1999). Arf proteins bind to mitotic kinesin-like protein 1 (MKLP1) in a GTP-dependent fashion. Cell Motil Cytoskel 44, 119–132.

Borowicz S, Van Scoyk M, Avasarala S, Karuppusamy Rathinam MK, Tauler J, Bikkavilli RK, Winn RA (2014). The soft agar colony formation assay. J Vis Exp 2014, e51998.

Bouchoux J, Beilstein F, Pauquai T, Guerrera IC, Chateau D, Ly N, Alqub M, Klein C, Chambaz J, Rousset M, *et al*. (2011). The proteome of cytosolic lipid droplets isolated from differentiated Caco-2/TC7 enterocytes reveals cell-specific characteristics. Biol Cell 103, 499–517.

Bowzard JB, Cheng D, Peng J, Kahn RA (2007). ELMOD2 is an Arl2 GTPase-activating protein that also acts on Arfs. J Biol Chem 282, 17568–17580.

Brugnera E, Haney L, Grimsley C, Lu M, Walk SF, Tosello-Trampont AC, Macara IG, Madhani H, Fink GR, Ravichandran KS (2002). Unconventional Rac-GEF activity is mediated through the Dock180-ELMO complex. Nat Cell Biol 4, 574–582.

Bugnard E, Zaal KJ, Ralston E (2005). Reorganization of microtubule nucleation during muscle differentiation. Cell Motil Cytoskel 60, 1–13.

Burd CG, Strochlic TI, Gangi Setty SR (2004). Arf-like GTPases: not so Arf-like after all. Trends Cell Biol 14, 687–694.

Cavenagh MM, Breiner M, Schurmann A, Rosenwald AG, Terui T, Zhang C, Randazzo PA, Adams M, Joost HG, Kahn RA (1994). ADP-ribosylation factor (ARF)-like 3, a new member of the ARF family of GTP-binding proteins cloned from human and rat tissues. J Biol Chem 269, 18937–18942.

Cavenagh MM, Whitney JA, Carroll K, Zhang C, Boman AL, Rosenwald AG, Mellman I, Kahn RA (1996). Intracellular distribution of Arf proteins in mammalian cells. Arf6 is uniquely localized to the plasma membrane. J Biol Chem 271, 21767–21774.

Chabin-Brion K, Marceiller J, Perez F, Settegrana C, Drechou A, Durand G, Pous C (2001). The Golgi complex is a microtubule-organizing organelle. Mol Biol Cell 12, 2047–2060.

Chipperfield RG, Jones SS, Lo KM, Weinberg RA (1985). Activation of Haras p21 by substitution, deletion, and insertion mutations. Mol Cell Biol 5, 1809–1813.

Cunningham LA, Kahn RA (2008). Cofactor D functions as a centrosomal protein and is required for the recruitment of the gamma-tubulin ring complex at centrosomes and organization of the mitotic spindle. J Biol Chem 283, 7155–7165.

Donaldson JG, Jackson CL (2011). ARF family G proteins and their regulators: roles in membrane transport, development and disease. Nat Rev Mol Cell Biol 12, 362–375.

Donaldson JG, Radhakrishna H (2001). Expression and properties of ADP-ribosylation factor (ARF6) in endocytic pathways. Methods Enzymol 329, 247–256.

D'Souza-Schorey C, Chavrier P (2006). ARF proteins: roles in membrane traffic and beyond. Nat Rev Mol Cell Biol 7, 347–358.

D'Souza-Schorey C, Li G, Colombo MI, Stahl PD (1995). A regulatory role for ARF6 in receptor-mediated endocytosis. Science 267, 1175–1178.

D'Souza-Schorey C, van Donselaar E, Hsu VW, Yang C, Stahl PD, Peters PJ (1998). ARF6 targets recycling vesicles to the plasma membrane: insights from an ultrastructural investigation. J Cell Biol 140, 603–616.

D'Souza RS, Lim JY, Turgut A, Servage K, Zhang J, Orth K, Sosale N, Lazzara M, Allegood J, Casanova JE (2020). Calcium-stimulated disassembly of focal adhesions mediated by an ORP3/IQSec1 complex. Elife 9, e54113.

East MP, Bowzard JB, Dacks JB, Kahn RA (2012). ELMO domains, evolutionary and functional characterization of a novel GTPase-activating protein (GAP) domain for Arf protein family GTPases. J Biol Chem 287, 39538–39553.

East MP, Kahn RA (2011). Models for the functions of Arf GAPs. Semin Cell Dev Biol 22, 3–9.

Efimov A, Kharitonov A, Efimova N, Loncarek J, Miller PM, Andreyeva N, Gleeson P, Galjart N, Maia AR, McLeod IX, *et al*. (2007). Asymmetric CLASP-dependent nucleation of noncentrosomal microtubules at the trans-Golgi network. Dev Cell 12, 917–930.

Fidyk N, Wang JB, Cerione RA (2006). Influencing cellular transformation by modulating the rates of GTP hydrolysis by Cdc42. Biochemistry 45, 7750–7762.

Fielding AB, Schonteich E, Matheson J, Wilson G, Yu X, Hickson GR, Srivastava S, Baldwin SA, Prekeris R, Gould GW (2005). Rab11-FIP3 and FIP4 interact with Arf6 and the Exocyst to control membrane traffic in cytokinesis. EMBO J 24, 3389–3399.

Francis JW, Goswami D, Novick SJ, Pascal BD, Weikum ER, Ortlund EA, Griffin PR, Kahn RA (2017a). Nucleotide binding to ARL2 in the TBCDARL2beta-tubulin complex drives conformational changes in beta-tubulin. J Mol Biol 429, 3696–3716.

Francis JW, Newman LE, Cunningham LA, Kahn RA (2017b). A trimer consisting of the tubulin-specific chaperone D (TBCD), regulatory GTPase ARL2, and beta-tubulin is required for maintaining the microtubule network. J Biol Chem 292, 4336–4349.

Francis JW, Turn RE, Newman LE, Schiavon C, Kahn RA (2016). Higher order signaling: ARL2 as regulator of both mitochondrial fusion and microtubule dynamics allows integration of 2 essential cell functions. Small GTPases 7, 188–196.

Frank SR, Hatfield JC, Casanova JE (1998). Remodeling of the actin cytoskeleton is coordinately regulated by protein kinase C and the ADP-ribosylation factor nucleotide exchange factor ARNO. Mol Biol Cell 9, 3133–3146.

Gillingham AK, Munro S (2007). The small G proteins of the Arf family and their regulators. Annu Rev Cell Dev Biol 23, 579–611.

Gumienny TL, Brugnera E, Tosello-Trampont AC, Kinchen JM, Haney LB, Nishiwaki K, Walk SF, Nemergut ME, Macara IG, Francis R, *et al*. (2001). CED-12/ELMO, a novel member of the CrkII/Dock180/Rac pathway, is required for phagocytosis and cell migration. Cell 107, 27–41.

Hanai A, Ohgi M, Yagi C, Ueda T, Shin HW, Nakayama K (2016). Class I Arfs (Arf1 and Arf3) and Arf6 are localized to the Flemming body and play important roles in cytokinesis. J Biochem 159, 201–208.

Hickson GRX, Matheson J, Riggs B, Maier VH, Fielding AB, Prekeris R, Sullivan W, Barr FA, Gould GW (2003). Arfophilins are dual Arf/Rab 11 binding proteins that regulate recycling endosome distribution and are related to Drosophila nuclear fallout. Mol Biol Cell 14, 2908–2920.

Hodgson U, Pulkkinen V, Dixon M, Peyrard-Janvid M, Rehn M, Lahermo P, Ollikainen V, Salmenkivi K, Kinnula V, Kere J, *et al*. (2006). ELMOD2 is a candidate gene for familial idiopathic pulmonary fibrosis. Am J Hum Genet 79, 149–154.

Horgan CP, McCaffrey MW (2009). The dynamic Rab11-FIPs. Biochem Soc Trans 37, 1032–1036.

Hosaka M, Toda K, Takatsu H, Torii S, Murakami K, Nakayama K (1996). Structure and intracellular localization of mouse ADP-ribosylation factors type 1 to type 6 (ARF1-ARF6). J Biochem 120, 813–819.

Hoyt MA, Stearns T, Botstein D (1990). Chromosome instability mutants of Saccharomyces cerevisiae that are defective in microtubule-mediated processes. Mol Cell Biol 10, 223–234.

Inoue H, Randazzo PA (2007). Arf GAPs and their interacting proteins. Traffic 8, 1465–1475.

Ismail SA, Chen YX, Rusinova A, Chandra A, Bierbaum M, Gremer L, Triola G, Waldmann H, Bastiaens PI, Wittinghofer A (2011). Arl2-GTP and Arl3-GTP regulate a GDI-like transport system for farnesylated cargo. Nat Chem Biol 7, 942–949.

Ivanova AA, East MP, Yi SL, Kahn RA (2014). Characterization of recombinant ELMOD (cell engulfment and motility domain) proteins as GTPase-activating proteins (GAPs) for ARF family GTPases. J Biol Chem 289, 11111–11121.

Jackson CL, Bouvet S (2014). Arfs at a glance. J Cell Sci 127, 4103–4109.

Johnson KR, Longo-Guess CM, Gagnon LH (2012). Mutations of the mouse ELMO domain containing 1 gene (Elmod1) link small GTPase signaling to actin cytoskeleton dynamics in hair cell stereocilia. PLoS One 7, e36074.

Kahn RA, Volpicelli-Daley L, Bowzard B, Shrivastava-Ranjan P, Li Y, Zhou C, Cunningham L (2005). Arf family GTPases: roles in membrane traffic and microtubule dynamics. Biochem Soc Trans 33, 1269–1272.
Klinger CM, Spang A, Dacks JB, Ettema TJ (2016). Tracing the archaeal origins of eukaryotic membrane-trafficking system building blocks. Mol Biol Evol 33, 1528–1541.
Kuriyama R, Dragas-Granoic S, Maekawa T, Vassilev A, Khodjakov A, Kobayashi H (1994). Heterogeneity and microtubule interaction of the CHO1 antigen, a mitosis-specific kinesin-like protein. Analysis of subdomains expressed in insect sf9 cells. J Cell Sci 107 (Pt 12), 3485–3499.
Li W, Feng Y, Chen A, Li T, Huang S, Liu J, Liu X, Liu Y, Gao J, Yan D, *et al.* (2019). Elmod3 knockout leads to progressive hearing loss and abnormalities in cochlear hair cell stereocilia. Hum Mol Genet 28, 4103–4112.
Li W, Sun J, Ling J, Li J, He C, Liu Y, Chen H, Men M, Niu Z, Deng Y, *et al.* (2018). ELMOD3, a novel causative gene, associated with human autosomal dominant nonsyndromic and progressive hearing loss. Hum Genet 137, 329–342.
Li Y, Kelly WG, Logsdon JM Jr, Schurko AM, Harfe BD, Hill-Harfe KL, Kahn RA (2004). Functional genomic analysis of the ADP-ribosylation factor family of GTPases: phylogeny among diverse eukaryotes and function in C. elegans. FASEB J 18, 1834–1850.
Lin R, Bagrodia S, Cerione R, Manor D (1997). A novel Cdc42Hs mutant induces cellular transformation. Curr Biol 7, 794–797.
Lin R, Cerione RA, Manor D (1999). Specific contributions of the small GTPases Rho, Rac, and Cdc42 to Dbl transformation. J Biol Chem 274, 23633–23641.
Loi E, Moi L, Blois S, Bacchelli E, Vega Benedetti AF, Cameli C, Fadda R, Maestrini E, Carta M, Doneddu G, Zavattari P (2020). ELMOD3-SH2D6 gene fusion as a possible co-star actor in autism spectrum disorder scenario. J Cell Mol Med 24, 2064–2069.
Lu M, Kinchen JM, Rossman KL, Grimsley C, deBakker C, Brugnera E, Tosello-Trampont AC, Haney LB, Klingele D, Sondek J, *et al.* (2004). PH domain of ELMO functions in trans to regulate Rac activation via Dock180. Nat Struct Mol Biol 11, 756–762.
Makyio H, Ohgi M, Takei T, Takahashi S, Takatsu H, Katoh Y, Hanai A, Ueda T, Kanaho Y, Xie Y, *et al.* (2012). Structural basis for Arf6-MKLP1 complex formation on the Flemming body responsible for cytokinesis. EMBO J 31, 2590–2603.
McElver J, Patton D, Rumbaugh M, Liu C, Yang LJ, Meinke D (2000). The TITAN5 gene of Arabidopsis encodes a protein related to the ADP ribosylation factor family of GTP binding proteins. Plant Cell 12, 1379–1392.
Miryounesi M, Bahari S, Salehpour S, Alipour N, Ghafouri-Fard S (2019). ELMO domain containing 1 (ELMOD1) gene mutation is associated with mental retardation and autism spectrum disorder. J Mol Neurosci 69, 312–315.
Mizuno-Yamasaki E, Rivera-Molina F, Novick P (2012). GTPase networks in membrane traffic. Annu Rev Biochem 81, 637–659.
Moravec R, Conger KK, D'Souza R, Allison AB, Casanova JE (2012). BRAG2/GEP100/IQSec1 interacts with clathrin and regulates alpha5beta1 integrin endocytosis through activation of ADP ribosylation factor 5 (Arf5). J Biol Chem 287, 31138–31147.
Muromoto R, Sekine Y, Imoto S, Ikeda O, Okayama T, Sato N, Matsuda T (2008). BART is essential for nuclear retention of STAT3. Int Immunol 20, 395–403.
Nahse V, Christ L, Stenmark H, Campsteijn C (2017). The abscission checkpoint: making it to the final cut. Trends Cell Biol 27, 1–11.
Nakayama K (2016). Regulation of cytokinesis by membrane trafficking involving small GTPases and the ESCRT machinery. Crit Rev Biochem Mol Biol 51, 1–6.
Newman LE, Schiavon CR, Turn RE, Kahn RA. (2017a). The ARL2 GTPase regulates mitochondrial fusion from the intermembrane space. Cell Logist 7, e1340104.
Newman LE, Schiavon CR, Zhou C, Kahn RA. (2017b). The abundance of the ARL2 GTPase and its GAP, ELMOD2, at mitochondria are modulated by the fusogenic activity of mitofusins and stressors. PLoS One 12, e0175164.
Newman LE, Zhou CJ, Mudigonda S, Mattheyses AL, Paradies E, Marobbio CM, Kahn RA (2014). The ARL2 GTPase is required for mitochondrial morphology, motility, and maintenance of ATP levels. PLoS One 9, e99270.
Nie Z, Hirsch DS, Randazzo PA (2003). Arf and its many interactors. Curr Opin Cell Biol 15, 396–404.
Nithianantham S, Le S, Seto E, Jia W, Leary J, Corbett KD, Moore JK, Al-Bassam J (2015). Tubulin cofactors and Arl2 are cage-like chaperones that regulate the soluble alphabeta-tubulin pool for microtubule dynamics. eLife 4, e08811.
Peterman E, Prekeris R (2019). The postmitotic midbody: regulating polarity, stemness, and proliferation. J Cell Biol 218, 3903–3911.
Petry S, Vale RD (2015). Microtubule nucleation at the centrosome and beyond. Nat Cell Biol 17, 1089–1093.
Price HP, Peltan A, Stark M, Smith DF (2010). The small GTPase ARL2 is required for cytokinesis in Trypanosoma brucei. Mol Biochem Parasitol 173, 123–131.
Prigent M, Dubois T, Raposo G, Derrien V, Tenza D, Rosse C, Camonis J, Chavrier P (2003). ARF6 controls post-endocytic recycling through its downstream exocyst complex effector. J Cell Biol 163, 1111–1121.
Pulkkinen V, Bruce S, Rintahaka J, Hodgson U, Laitinen T, Alenius H, Kinnula VL, Myllarniemi M, Matikainen S, Kere J (2010). ELMOD2, a candidate gene for idiopathic pulmonary fibrosis, regulates antiviral responses. FASEB J 24, 1167–1177.
Radcliffe PA, Vardy L, Toda T (2000). A conserved small GTP-binding protein Alp41 is essential for the cofactor-dependent biogenesis of microtubules in fission yeast. FEBS Lett 468, 84–88.
Radhakrishna H, Donaldson JG (1997). ADP-ribosylation factor 6 regulates a novel plasma membrane recycling pathway. J Cell Biol 139, 49–61.
Randazzo PA, Inoue H, Bharti S (2007). Arf GAPs as regulators of the actin cytoskeleton. Biol Cell 99, 583–600.
Reinstein J, Schlichting I, Frech M, Goody RS, Wittinghofer A (1991). p21 with a phenylalanine 28 → leucine mutation reacts normally with the GTPase activating protein GAP but nevertheless has transforming properties. J Biol Chem 266, 17700–17706.
Rios RM (2014). The centrosome Golgi apparatus nexus. Philos Trans R Soc Lond B Biol Sci 369, 20130462.
Sankaran S, Starita LM, Groen AC, Ko MJ, Parvin JD (2005). Centrosomal microtubule nucleation activity is inhibited by BRCA1-dependent ubiquitination. Mol Cell Biol 25, 8656–8668.
Santy LC (2002) Characterization of a fast cycling ADP-ribosylation factor 6 mutant. J Biol Chem 277, 40185–40188.
Santy LC, Ravichandran KS, Casanova JE (2005). The DOCK180/Elmo complex couples ARNO-mediated Arf6 activation to the downstream activation of Rac1. Curr Biol 15, 1749–1754.
Schiavon CR, Griffin ME, Pirozzi M, Parashuraman R, Zhou W, Jinnah HA, Reines D, Kahn RA (2018). Compositional complexity of rods and rings. Mol Biol Cell 29, 2303–2316.
Schiavon CR, Turn RE, Newman LE, Kahn RA (2019). ELMOD2 regulates mitochondrial fusion in a mitofusin-dependent manner, downstream of ARL2. Mol Biol Cell 30, 1198–1213.
Schiel JA, Simon GC, Zaharris C, Weisz J, Castle D, Wu CC, Prekeris R (2012). FIP3-endosome-dependent formation of the secondary ingression mediates ESCRT-III recruitment during cytokinesis. Nat Cell Biol 14, 1068–1078.
Schlacht A, Mowbrey K, Elias M, Kahn RA, Dacks JB (2013). Ancient complexity, opisthokont plasticity, and discovery of the 11th subfamily of Arf GAP proteins. Traffic 14, 636–649.
Schonteich E, Pilli M, Simon GC, Matern HT, Junutula JR, Sentz D, Holmes RK, Prekeris R (2007). Molecular characterization of Rab11-FIP3 binding to ARF GTPases. Eur J Cell Biol 86, 417–431.
Schweitzer JK, D'Souza-Schorey C (2002). Localization and activation of the ARF6 GTPase during cleavage furrow ingression and cytokinesis. J Biol Chem 277, 27210–27216.
Schweitzer JK, D'Souza-Schorey C (2005). A requirement for ARF6 during the completion of cytokinesis. Exp Cell Res 311, 74–83.
Schweitzer JK, Sedgwick AE, D'Souza-Schorey C (2011). ARF6-mediated endocytic recycling impacts cell movement, cell division and lipid homeostasis. Semin Cell Dev Biol 22, 39–47.
Seixas E, Barros M, Seabra MC, Barral DC (2013). Rab and Arf proteins in genetic diseases. Traffic 14, 871–885.
Sharer JD, Kahn RA (1999). The ARF-like 2 (ARL2)-binding protein, BART. Purification, cloning, and initial characterization. J Biol Chem 274, 27553–27561.
Sharer JD, Shern JF, Van Valkenburgh H, Wallace DC, Kahn RA (2002). ARL2 and BART enter mitochondria and bind the adenine nucleotide transporter. Mol Biol Cell 13, 71–83.
Shiba T, Koga H, Shin HW, Kawasaki M, Kato R, Nakayama K, Wakatsuki S (2006). Structural basis for Rab11-dependent membrane recruitment of a family of Rab11-interacting protein 3 (FIP3)/arfophilin-1. Proc Natl Acad Sci USA 103, 15416–15421.
Shultz T, Shmuel M, Hyman T, Altschuler Y (2008). Beta-tubulin cofactor D and ARL2 take part in apical junctional complex disassembly and abrogate epithelial structure. FASEB J 22, 168–182.

Song J, Khachikian Z, Radhakrishna H, Donaldson JG (1998). Localization of endogenous ARF6 to sites of cortical actin rearrangement and involvement of ARF6 in cell spreading. J Cell Sci 111 (Pt 15), 2257–2267.
Spang A, Shiba Y, Randazzo PA (2010). Arf GAPs: gatekeepers of vesicle generation. FEBS Lett 584, 2646–2651.
Stearns T, Hoyt MA, Botstein D (1990). Yeast mutants sensitive to antimicrotubule drugs define three genes that affect microtubule function. Genetics 124, 251–262.
Steinborn K, Maulbetsch C, Priester B, Trautmann S, Pacher T, Geiges B, Kuttner F, Lepiniec L, Stierhof YD, Schwarz H, *et al.* (2002). The Arabidopsis PILZ group genes encode tubulin-folding cofactor orthologs required for cell division but not cell growth. Genes Dev 16, 959–971.
Suzuki M, Murakami T, Cheng J, Kano H, Fukata M, Fujimoto T (2015). ELMOD2 is anchored to lipid droplets by palmitoylation and regulates adipocyte triglyceride lipase recruitment. Mol Biol Cell 26, 2333–2342.
Sztul E, Chen PW, Casanova JE, Cherfils J, Dacks JB, Lambright DG, Lee FS, Randazzo PA, Santy LC, Schurmann A, *et al.* (2019). ARF GTPases and their GEFs and GAPs: concepts and challenges. Mol Biol Cell 30, 1249–1271.
Takahashi S, Takei T, Koga H, Takatsu H, Shin HW, Nakayama K (2011). Distinct roles of Rab11 and Arf6 in the regulation of Rab11-FIP3/arfophilin-1 localization in mitotic cells. Genes Cells 16, 938–950.
Tassin AM, Maro B, Bornens M (1985a). Fate of microtubule-organizing centers during myogenesis in vitro. J Cell Biol 100, 35–46.
Tassin AM, Paintrand M, Berger EG, Bornens M (1985b). The Golgi apparatus remains associated with microtubule organizing centers during myogenesis. J Cell Biol 101, 630–638.
Tian G, Huang Y, Rommelaere H, Vandekerckhove J, Ampe C, Cowan NJ (1996). Pathway leading to correctly folded beta-tubulin. Cell 86, 287–296.
Tian G, Thomas S, Cowan NJ (2010). Effect of TBCD and its regulatory interactor Arl2 on tubulin and microtubule integrity. Cytoskeleton (Hoboken) 67, 706–714.
Tulu US, Fagerstrom C, Ferenz NP, Wadsworth P (2006). Molecular requirements for kinetochore-associated microtubule formation in mammalian cells. Curr Biol 16, 536–541.
Ueda T, Hanai A, Takei T, Kubo K, Ohgi M, Sakagami H, Takahashi S, Shin HW, Nakayama K (2013). EFA6 activates Arf6 and participates in its targeting to the Flemming body during cytokinesis. FEBS Lett 587, 1617–1623.
Van Valkenburgh H, Shern JF, Sharer JD, Zhu X, Kahn RA (2001). ADP-ribosylation factors (ARFs) and ARF-like 1 (ARL1) have both specific and shared effectors: characterizing ARL1-binding proteins. J Biol Chem 276, 22826–22837.
Vitali T, Girald-Berlingeri S, Randazzo PA, Chen PW (2019). Arf GAPs: a family of proteins with disparate functions that converge on a common structure, the integrin adhesion complex. Small GTPases 10, 280–288.
Watzlich D, Vetter I, Gotthardt K, Miertzschke M, Chen YX, Wittinghofer A, Ismail S (2013). The interplay between RPGR, PDEdelta and Arl2/3 regulate the ciliary targeting of farnesylated cargo. EMBO Rep 14, 465–472.
Wilson GM, Fielding AB, Simon GC, Yu X, Andrews PD, Hames RS, Frey AM, Peden AA, Gould GW, Prekeris R (2005). The FIP3-Rab11 protein complex regulates recycling endosome targeting to the cleavage furrow during late cytokinesis. Mol Biol Cell 16, 849–860.
Wu J, Akhmanova A (2017). Microtubule-organizing centers. Annu Rev Cell Dev Biol 33, 51–75.
Zhang CJ, Bowzard JB, Anido A, Kahn RA (2003). Four ARF GAPs in Saccharomyces cerevisiae have both overlapping and distinct functions. Yeast 20, 315–330.
Zhang CJ, Cavenagh MM, Kahn RA (1998). A family of Arf effectors defined as suppressors of the loss of Arf function in the yeast Saccharomyces cerevisiae. J Biol Chem 273, 19792–19796.
Zhang CJ, Rosenwald AG, Willingham MC, Skuntz S, Clark J, Kahn RA (1994). Expression of a dominant allele of human ARF1 inhibits membrane traffic in vivo. J Cell Biol 124, 289–300.
Zhou C, Cunningham L, Marcus AI, Li Y, Kahn RA (2006). Arl2 and Arl3 regulate different microtubule-dependent processes. Mol Biol Cell 17, 2476–2487.
Zhou CX, Shi LY, Li RC, Liu YH, Xu BQ, Liu JW, Yuan B, Yang ZX, Ying XY, Zhang D (2017). GTPase-activating protein Elmod2 is essential for meiotic progression in mouse oocytes. Cell Cycle 16, 852–860.
Zhu X, Kaverina I (2013). Golgi as an MTOC: making microtubules for its own good. Histochem Cell Biol 140, 361–367.